Miguel Ângelo Gomes Baeta

Licenciado em Ciências da Engenharia Física

Development of a cold stage for a 80 K vibration-free cooler

Dissertação para obtenção do Grau de Mestre em

Engenharia Física

Orientador: Prof. Dr. Grégoire Bonfait,
Professor Associado com Agregação,
Universidade Nova de Lisboa

Júri

Presidente: Prof. Dr. Filipe de Oliveira
Arguentes: Prof. Dr. Daniel Vaz
Prof. Dr. Grégoire Bonfait

FACULDADE DE CIÊNCIAS E TECNOLOGIA
UNIVERSIDADE NOVA DE LISBOA

September, 2016

Development of a cold stage for a 80 K vibration-free cooler

Este documento foi gerado utilizando o processador (pdf)LaTeX, com base no template "unlthesis" [1] desenvolvido no Dep. Informática da FCT-NOVA [2].
[1] https://github.com/joaomlourenco/unlthesis [2] http://www.di.fct.unl.pt

Acknowledgements

A realização desta tese de dissertação não teria sido possível sem o apoio recebido de forma direta ou indireta por parte de um conjunto de pessoas e entidades. Neste sentido, gostaria de expressar o meu profundo agradecimento nas linhas.

Em primeiro lugar gostaria de agradecer ao Professor Grégoire Bonfait pela oportunidade que me foi conferida e pela sua excelente orientação, tempo e dedicação despendidos.

Agradeço também aos meus colegas do laboratório de Criogenia: Patrícia Sousa, Hugo Rações, Mário Xavier, Diogo Silva, Sofia Alves e com especial destaque para o Jorge Barreto por me terem acompanhado e ajudado no desenvolvimento deste projeto.

Expresso também o meu agradecimento à oficina do departamento, ao Faustino e Eduardo, pela sua assistência e paciência na construção deste projeto.

Agradeço ainda à *Active Space Technologies* pela sua colaboração, bem como a todos os elementos desta empresa que participaram neste projeto.

Aqui expresso também o meu agradecimento à gloriosa Faculdade de Ciências e Tecnologias da Universidade Nova de Lisboa pelos fantásticos 5 anos que conduziram a este momento.

Para concluir, quero deixar aqui um enorme agradecimento à minha família em particular ao meus pais, Isabel Baeta e Paulo Baeta, seu apoio incondicional e esforço para me proporcionarem esta oportunidade. E também um muito obrigado aos meus amigos com destaque para a minha melhor amiga e namorada Inês Maldonado pela força e paciência ao longo desta jornada.

Muito obrigado a todos

Abstract

Nowadays, many satellites are observing the earth for many purposes (climatology, agriculture, defence and security, etc.) using infrared sensors. One of the key element of these sensors is their high resolution obtained due to their quite low operating temperature provided by mechanical cryocoolers.

However, the introduction of vibrations by the most of the cryocoolers is a recurring problem for space applications, and because of that the development of a system that eliminates these vibrations is very important. So, in the framework of a European Space agency project, a *40-80 K vibration-free cooler* is being developed that combines two cryocoolers (one that uses Nitrogen that precool another cryocooler that uses Neon), functioning without introducing vibrations in the system.

This thesis is focused on the nitrogen cryocooler more specifically on the dimensioning and development of its cold part's components as the Joule-Thomson valve, the counterflow heat exchanger, and its test systems.

The majority of the work on this thesis was focused on the design of the Joule-Thomson (JT) valve. Since Its dimensions and properties are empirically obtained, an extended experimental study of the performance of two different JT valves under several temperatures, pressures and mass flow conditions was made. The data obtained allowed us to dimension a JT valve for the required conditions and also confirm the operating principles of the cryocooler cold part.

The counterflow heat exchanger was dimensioned, built and integrated in a Gifford-Mac Mahon cryocooler and is ready to be tested as soon as the Joule Thomson valve is determined.

Keywords: cryogenics, vibration-free cooler, Joule-Thomson, counter-flow heat exchanger

Resumo

Atualmente são inúmeros os satélites que se encontram em observação da Terra, com as mais diversas finalidades (climatologia, agricultura, defesa e segurança, etc.), através do recurso a sensores infravermelhos. Um dos elementos chave destes sensores é a sua alta resolução, esta é obtida devido à sua temperatura de operação bastante baixa, o que é conseguido através da ação de criorefrigeradores mecânicos.

Contudo, a introdução de vibrações por parte da maioria dos criorefrigeradores constitui um problema recorrente na área da aeroespacial sendo pertinente o desenvolvimento de um equipamento que permita eliminar estas vibrações. Assim, encontra-se a ser desenvolvido no contexto de um projeto da Agência Espacial Europeia, o *40-80 K vibration-free cooler* que combina dois criorefrigeradores, um primeiro que utiliza Azoto que pré-arrefece um outro que utiliza Néon, e que desempenha a sua função sem, no entanto, introduzir vibração no sistema.

Esta tese incidiu no criorefrigerador de azoto, mais especificamente no dimensionamento e desenvolvimento de componentes do seu dedo frio como a válvula de Joule-Thomson, permutador de calor de contracorrente e respetivos sistemas de teste.

Foi sobre o dimensionamento da válvula de Joule-Thomson que recaíram a maior parte dos testes realizados, uma vez que este é um tema pouco estudado e que implicou o conhecimento e validação dos princípios de funcionamento desta válvula, temperatura, potência frigorífica e fluxo de massa. Após a realização destes testes, conseguiu-se dimensionar a válvula e ainda comprovar os princípios de funcionamento do dedo frio.

O permutador de calor contracorrente foi dimensionado, construído e integrado no criorefrigerador Gifforf- Mac Mahon, e encontra-se pronto a ser testado, logo que a válvula de Joule Thomson esteja terminada.

Palavras-chave: criogenia, criorefrigerador sem vibrações, Joule-Thomson, permutador de calor de contracorrente

Contents

List of Figures

List of Tables

Chapter 1

Introduction

In the last years the requirements of the technologies used in space missions have been increasing, which led to the need to improve their performances. In several areas such as detection systems, telecommunications, conservation of samples, etc., this efficiency can be achieved with the assistance of autonomous cryogenic systems, called coolers, to replace the use of cryogenic liquids. Unfortunately, these systems have some disadvantages: for instance, for highly sensitive detection systems, their biggest disadvantage is the introduction of vibrations produced by mechanical compressors, which may cause a decrease of the system quality.

In an attempt to eliminate this problem, European Space Agency (ESA) proposed the development of a 40-80 K vibration-free cooler. One of the two winning proposals was assigned in 2015 to a consortium grouping: a Portuguese company - Active Space Technologies (a company based in Coimbra, that works in di fferent areas, such as space, aeronautics, nuclear, defense, industry and research), the Cryogenics Laboratory from LIBPhys and the Laboratory of Adsorption Technology & Process Engineering (LATPE, REQUIMTE), both located at the Faculdade de Ciências e Tecnologias, Universidade Nova de Lisboa.

The objectives of this project are the design, construction and validation of a two-stage vibration free cooler, using nitrogen and neon as the working fluids and a Joule-Thonson expansion as cooling source. The cold part of this system, as depicted inside the dashed box on picture 1.1, consists on counterflow heat exchangers, and Joule-Thomson valves. Attached to the cold part is a gas manifold for the gas management and a set of adsorption cells acting as thermal compressors.

With the development of this project it is expected in the nitrogen cooler a low temperature, around 80 K, with a cold power of 1.5 W, so that in a second phase of this project this system can pre-cool the neon sorption cryocooler in order to reach temperatures

around 40 K, with a cold power of 0.5 W. These two cryocoolers form a vibrationless system due to the absence of moving parts. In the future, the whole system can cool an infrared device for Earth observations in ESA space missions.

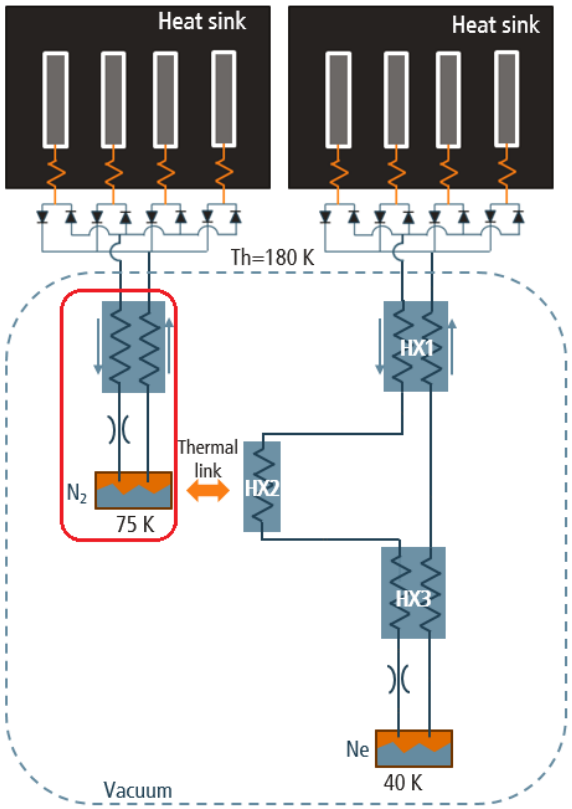

Figure 1.1: Schematic of the vibration free cooler to be developed in the framework of an ESA project entitled "Development of a 40-80 K vibration free cryocooler" proposal, AST-FCT, 2014

It is in the framework of this project that this master thesis is included. The work will be focused on developing the first version of the cold part of the vibration free cooler using nitrogen, with a low temperature around 80 K and a cold power of 1.5 W, represented inside the red box on picture 1.1. More specifically, it includes the design and construction of the counterflow heat exchanger and the Joule-Thomson valve. It includes also, the construction of a system to test the operation of the componements and the system requirements.

In the next chapter 2, some vibration free coolers are presented, as also some of their performances and applications, in chapter 3 is described the adopted solutions for the 80 K cold stage, that satisfied the requirements made by ESA in the framework of this project, the experimental setup built is then described in chapter 4 and the results obtained in chapter 5, with the respective discussion. To finish, the conclusions of this work are summarized in Chapter 6.

CHAPTER 2

VIBRATION FREE COOLERS

In this chapter are presented different types of cryocoolers , some of their performances and limitations are compared as well as the most common applications in order to justify the choice of a Joule-Thomson system.

2.1 Coolers usually used in satellites

The coolers can be divided in two groups, passive and active coolers. The passive coolers do not require an electric power supply and have been extensively used in space applications due to their high reliability and low vibrations level.

The active coolers, also called cryocoolers, in contrast with passive coolers, require electrical power. This energy is used to provide work to a closed thermodynamic cycle, which allows the heat absorption and consequent cooling at the "cold finger" level. The work is usually done by a mechanical compressor, which causes vibration in this system and is therefore the biggest disadvantage in some systems. These coolers may also have multiple stages in order to achieve lower temperatures.

The first active cooler successfully operated in space was a Stirling cycle machine to cool two gamma ray detectors, launched in 1978 and developed by Phillips[1].

In addition, as opposed to passive coolers, the active coolers may cover all ranges of temperatures and can work at any orbit.

2.1.1 Passive Coolers

- Radiators

  They are composed by multiple panels that emit heat in the form of radiation, according to Stefan - Boltzmann's law. Each panel represents a stage and the temperature is decreased along these stages, with a low temperature limit around 70

K in the most cases. Beyond their passive characteristic, another main advantage of these systems is their lifetime because their only limitation is the degradation of the surface of the panels, which is, in space very slow. Their major drawbacks is their limiting temperature and their relatively low cooling power below ≈100 K. Moreover, in the case of radiators in orbits nearby Earth it is difficult to reach temperatures below $70\ K$.

- Cryogenic liquids

  The working principle of this type of coolers is quite simple. It consists in a liquid reservoir (Dewar) where the heat dissipated by the sensors is transferred to the fluid by keeping objects dipped in the liquid or in thermal contact with the reservoir at temperatures near the boiling temperature of the fluid. The cryogenic liquids are very suitable due to their temperature stability and their simplicity, although they have a main disadvantage, the fact of adding large weight and volume to the system and of having a finite life time associated with the amount of stored fluid. Let us note that many temperature ranges, in particular the 44 - 54 K, are not covered by this type of coolers, due to the absence of pure liquid fluids in that temperature range.

2.1.2 Active Coolers

- Stirling cycle

  They are constituted by a compressor and a regenerative heat exchanger, in general, displaceable, also known as regenerator-displacer. This system is known as the Stirling cycle, which consists of two isochoric processes and two isothermal processes [1].

- Pulse tube

  The Pulse tube cryocooler is also constituted by a compressor, but, in opposite to the Stirling machine, the regenerator is fixed. This fact eliminates all the moving parts at low temperatures and makes these cryocoolers mechanically simpler and with a low level of vibrations at the cold finger. However, it is difficult to achieve high efficiencies close to the values of Stirling in this type of system.

- Joule-Thomson

  The principle of these cryocoolers is based on the Joule-Thomson effect which corresponds to an isenthalpic expansion that occurs when a gas is forced to pass through a small restriction with the assistance of a mechanical compressor. Below the inversion temperature, that is gas dependent, this expansion leads to a cooling. However, this process is highly irreversible which makes these cryocoolers relatively inefficient when compared to the previous two, but highly reliable due to its simplicity

(absence of moving parts at low temperature) and because low temperature can be achieved using adequate cryogenic fluids.

- Joule-Thomson sorption coolers

  The sorption coolers systems are similar to the Joule-Thomson ones, and are constituted by the same components except the source of gas flow: the mechanical compressor is replaced by adsorption or absorption cells. The cells are volumes filled by adsorption or absorption materials, such as activated carbon or metal hydrides, respectively. When these materials are cooled the gas particles are retained (in surface or in volume) by the material by physical processes, as Van der Waals forces, or chemical processes, usually covalent bonds. When they are heated the particles are released providing the necessary pressure to the system. These cryocoolers have a great potential, in spite of having a relatively low efficiency, because when the mechanical compressor is replaced, all moving parts of the system are eliminated and consequently also their inherent vibrations. It is a cryocooler of this type that will be developed in this project.

Table 2.1: Table of cryocoolers often used below 100 K in space cryogenics adapt from [1]

Parameters of coolers			
Cooler	Temperature	Advantages	Disadvantages
Radiator	80 K	Reliable, low vibration, long lifetime	Complicates in orbits nearby Earth
Cryogenic liquids	1.8 K	Stable, low vibration	Short lifetime, complex, out-gassing, massive
Stirling	80 K to 20 K	Efficient, intermediate temperature	Vibrations
Pulse tube	80 K	Lower vibrations	Lower efficiency, than Stirling
Joule-Thomson	4 K	Low vibrations	Low eficiency
Sorption	10 K	Very low vibrations	Low eficiency

2.1.3 Joule-Thomson sorption coolers: general principles

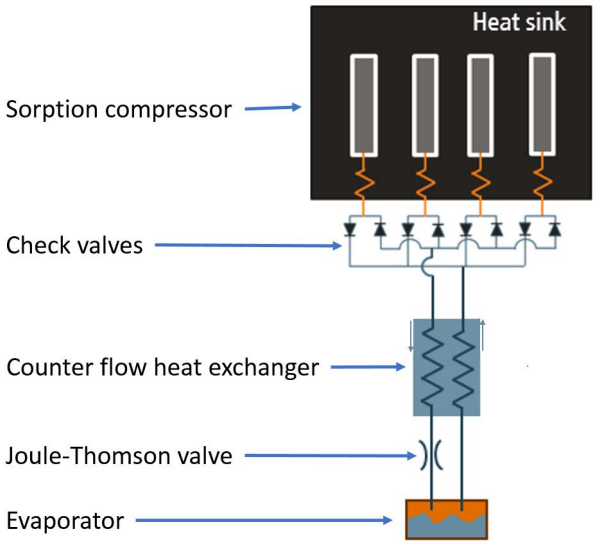

Figure 2.1: Schematic of a sorption cooler

The operation of the Joule-Thomson sorption coolers is schematized in figure 2.1 and can be divided in several steps:

- Gas supply

  The material constituting the absorption cell is the key to the sorption compressor operation. This should be capable of absorbing large amounts of gas at low pressure and temperature, and then desorb it when heated, thus providing the high pressure and the mass flow needed by the system. The temperature cycles are made using a heat switch, an electric heater and a heat sink (Radiator, Cryogenic liquid, etc.). When it is necessary to heat the cell, this should be kept thermally isolated (Heat switch open), to cool it is only necessary to couple the cell to the radiator (Heat switch closed), for example. The problem of using a single cell is that it does not provide a continuous cooling due to the adsorption-desorption steps that are necessary to provide the flow in a cyclic way. This problem can be solved by using multiple cells out of phase: through this principle and using one-way valves (check valves) it was possible to maintain a almost constant flow.

- Gas precooler

  After leaving the compressor, in first place, the high pressure gas flow is normally precooled with the assistance of the heat sink and then passes through several heat exchangers (counterflow heat exchangers) in order to cool the fluid to a desired temperature at the entry of the Joule-Thomson valve.

- Joule-Thomson valve

  After this pre-cooling, the gas flow is forced through a restriction valve, Joule-Thomson valve, which causes an isenthalpic expansion and consequently a decrease in the temperature and, in general, liquefaction of part of the fluid.

- Evaporator or Cold finger

  After the Joule-Thomson valve, a part of the cold fluid pass into the liquid state and is stored in a Liquid Reservoir, being in this location the lowest temperature of the cryocooler which corresponds to the evaporation temperature of the fluid. Liquid Reservoir is also where the heat is transfer to the device and this heat will cause the liquid evaporation. The gas will then return to the compressor by the low pressure side, through the several heat exchangers to be compressed again. That is why this system is a closed cycle and continuous.

2.2 Applications

2.2.1 Planck

The Planck satellite refers to a space mission that ESA launched on 14th May 2009, with the duration of three years. The purpose of this mission was to study the expansion of the universe by measuring with high precision the anisotropy of microwave radiation on space background.

The microwave measuring system was designed to measure frequencies between 30 and 957 GHz. To cover this frequency range it was necessary to divide the system in two devices, one for lower frequencies and another for high frequencies. To obtain the sensitivity required, the system had to be cooled[2]. For the low frequency device, the required minimum temperature was 20 K. Therefore, it was necessary to take particular care in the selection of the cryocooler to achieve these temperatures, due to the high sensitivity of the sensors. It was important that the cryocooler did not induce vibrations.

To solve this problem, the Jet Propulsion Laboratory (JPL) developed a redundant system with two sorption coolers with hydrogen as the working fluid, being this redundancy justified by the fact that the low frequency device was not the only one that was depended on those cryocoolers. They were designed to provide a cooling power around 1 Watt, 80% of this cooling power was used to cool the Low-Frequency Instrument (LFI). The other 20% were used to pre-cool the fluid used in two others cryogenics refrigerators (He J-T cooler to 4 K and Dilution cooler to 0.1 K) that maintain the High-Frequency Instrument (HFI) at 100 mK[3].

All these cryocoolers also depend on a radiator with three panels (V-groove arrangement) that is responsible for passive cooling to a temperature between 50 and 60 K.[4] A schematic of the Planck cooler is displayed in figure 2.2.

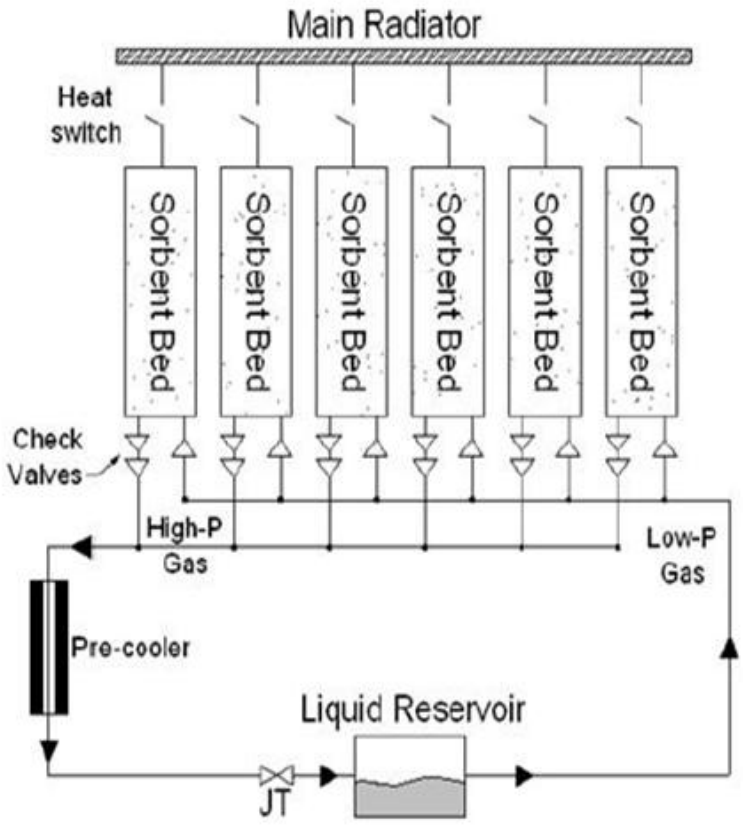

Figure 2.2: Sorption cooler from Planck[3]

2.2.2 METIS

As mentioned above, when we want to achieve very high resolution on a system, the utilization of a cryocooler is necessary, and the METIS instrument (Multi Element Telescope for Imaging and Spectroscopy), belonging to the European Organization for Astronomical Research in the Southern Hemisphere (ESO), is not an exception. The METIS is part of a group of several devices that belongs to the European Extremely Large Telescope (E-ELT), a very advanced telescope that will allow great advances in astrophysics (operation foreseen for 2024)

Just to have an idea of their dimensions, the E-RLT has a primary lens with 39 m of diameter and allows the capture of 15 times more light than the current telescopes. The METIS is a device that allows the analysis of infrared radiation with wavelengths between 3 and 14 μm.

This range may be divided into bands, the L band 3 to 4 μm, M band of 4.6 to 5 μm and N band of 7.5 to 14.5 μm. A device with this sensitivity cannot be affected by vibrations, therefore the use of cryocoolers with moving parts is unadvised: sorption cooler could be a solution. Until now, the cryocoolers have been developed by the University of Twente in collaboration with Dutch Space [5].

The METIS system uses a 3 sorption cryocoolers with different temperature ranges:

- Cryocooler 40 K

  It is constituted by a set of adsorption cells, a counterflow heat exchanger and Joule-Thomson valve restriction. The adsorption material of the cells of this cryocooler and the remaining cryocoolers are constituted by *Saran Carbon*. This cryocooler uses neon as the working fluid and is responsible for cooling the detection part of the wavelengths in bands L and M and acts as a pre-cooling stage for the two others cryocoolers.

- Cryocooler 25-15 K

  This one uses hydrogen and is constituted by two sets of adsorption cells because it requires a high pressure higher than 20 bar. Also uses 3 counterflow heat exchangers and two Joule-Thomson valves, the first provides a temperature of 25 K in order to cool the device of image forming from wavelengths in the N band, and the second Joule-Thomson valve allows the fluid to cool until the 15 K, necessary to pre-cool the 8 K cryocooler.

- Cryocooler 8 K

  The coldest stage uses Helium as the working fluid and is associated to the part of wavelengths detection in band N. It is constituted by one set of adsorption cells, 4 counterflow heat exchangers and one Joule-Thomson valve. In addition to the heat exchangers are also 3 others heat exchangers in contact with the remaining cryocoolers, at the temperatures of 40 K, 25 K and 15 K. These exchangers are essential for the cryocooler efficiency because the desired temperature is very sensitive to the inlet temperature of the Joule-Thomson valve. For instance, if the helium is not at the temperature of 15 K, at its entry, it turns to be impossible to achieve 8 K because the helium is not in the liquid state after the JT expansion (supercritical state).

All of the adsortion cells are precooled using a reservoir of liquid nitrogen at a temperature around 85K[5].

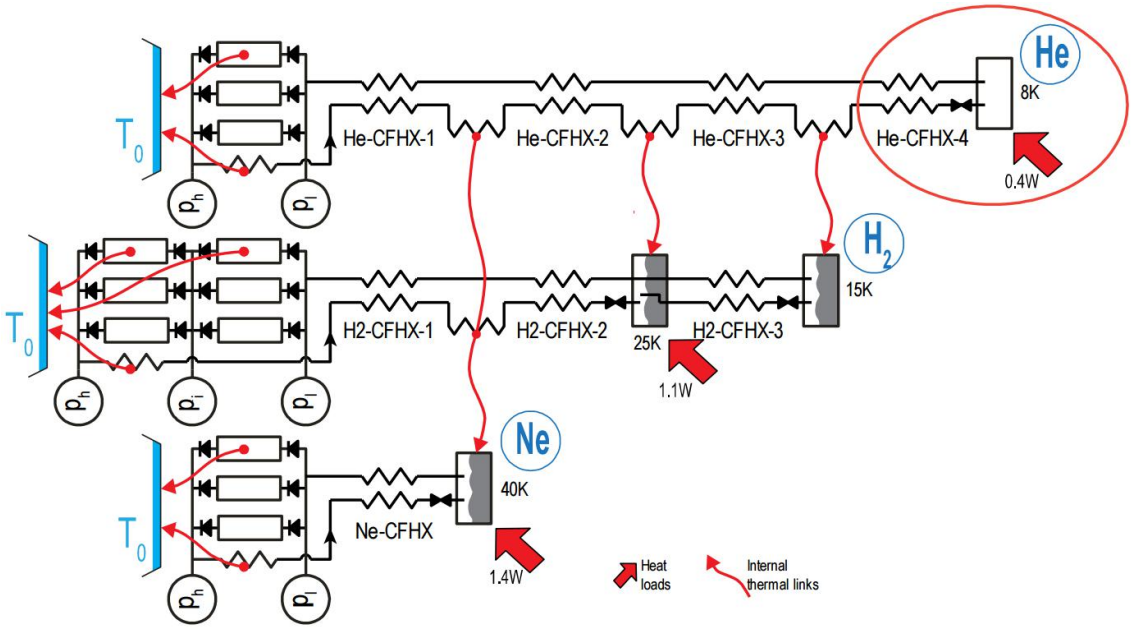

Figure 2.3: Sorption coolers system from METIS[5]

CHAPTER 3

THERMAL AND MECHANICAL REQUIREMENTS AND ADOPTED SOLUTION

3.1 Thermodynamic analysis of the cold part

To dimension the low temperature part of the N_2 system (Counterflow heat exchanger and Joule-Thomson valve), a thermodynamic analysis is needed. Its components are represented in the schematic of figure 3.1, as well as the indication of various points of interest in such system.

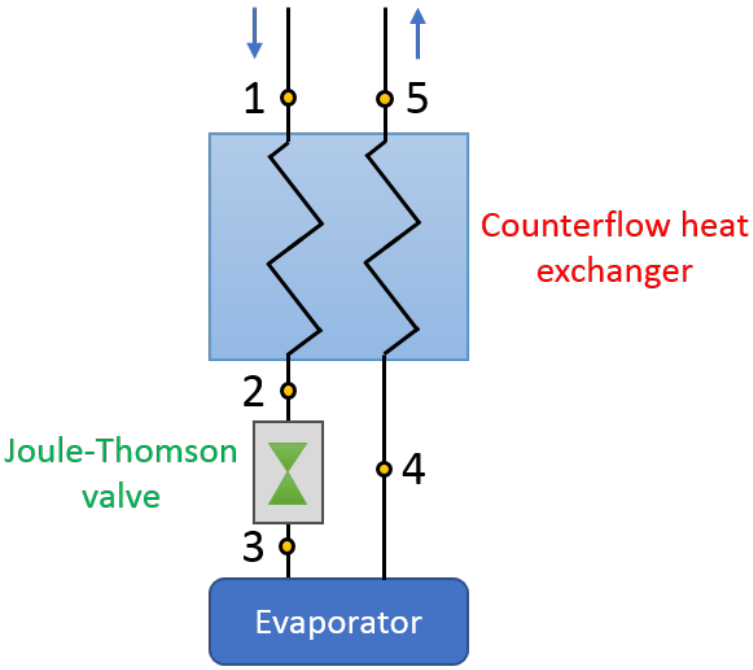

Figure 3.1: Nitrogen cold stage

With this system is expected a cooling power of 1.5 W at 80 K, from the initial conditions:

$$T_1 = 180\ K; \quad T_4 = 80\ K; \quad P_1 = 100\ bar.$$

The temperature T_1 is the temperature after heat sink (as explained in chapter 2.1.3) and is one of the requirements of ESA. When designing these type of systems, it is necessary to be aware of the processes that occur along the fluid path. These are represented in a PH diagram in figure 3.2 and described in the text below.

- Point 1 to 2, The pressure is constant (≈100 bars), isobaric process; The fluid is cooled by crossing the hot side of the heat exchanger that is in contact with the cold side.
- Point 2 to 3, the JT isenthalpic expansion takes place. The fluid is forced through the Joule-Thomson valve, it occurs a substantial temperature drop, and if T_2 is low enough, part of the fluid passes to the liquid state.
- Point 3 to 4, the temperature (80 K) and pressure are constant and equal to the saturation pressure of nitrogen at 80 K (≈ 1.5 bar). This is where the heat is dissipated by evaporation of the liquid nitrogen at constant temperature as far as the output pressure that is kept constant (let us remind that this pressure is mainly imposed by the adsorption cell).
- Point 4 to 5, the pressure is constant, isobaric process; The fluid temperature increases by exchanging the heat with the hot side of heat exchanger. In an ideal heat exchanger, and if $c_{p\ hot} > c_{p\ cold}$, T_5 reaches T_1 (180 K in our case)[6].

Table 3.1: System conditions

$P_1 = P_2 = 100bar$	$P_3 = P_4 = P_5 = 1.5bar$
$T_1 = T_5 = 180K$	$T_3 = T_4 = 80K$
$H_2 = H_3$	

The diagram of figure 3.2 also allows to determinate the liquid fraction, x_{liq}:

$$x_{liq} = \frac{(H_{liq} - H_3)}{(H_{gas} - H_{liq})} \tag{3.1}$$

The H_{liq} is the liquid saturation enthalpy and H_{gas} the vapor saturation enthalpy, equals to H_4.

At 80 K the value obtained is,

$$x_{liq} = 67.3\%$$

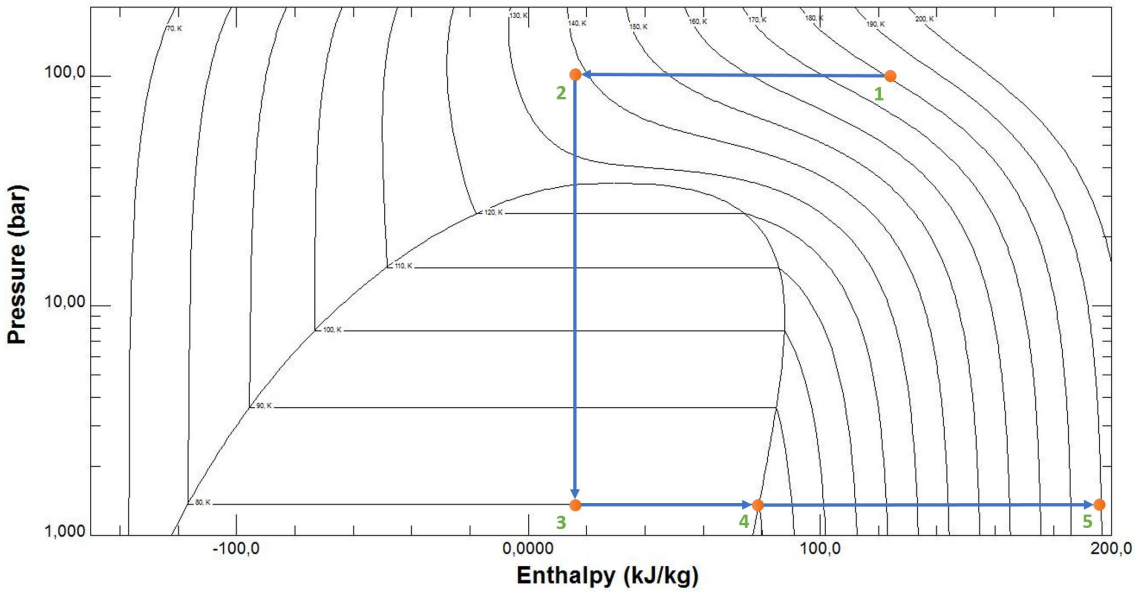

Figure 3.2: Thermodynamic processes in a PH diagram. The various steps are explained in the text.

Knowing that a 1.5 W cooling power ($\dot{Q}$) is needed, it is possible to estimate the gas flow required for the system.

$$\dot{Q} = \dot{m}L = \dot{m}(H_4 - H_3) \tag{3.2}$$

L being the latent heat of vaporization. This results in the following nitrogen mass flow

$$\dot{m} = 23.7\ mg/s$$

It is very important to know this mass flow of nitrogen in the system before designing any component, because this it is essential for the components dimensioning.

3.2 Counterflow heat exchanger

The counterflow heat exchanger (figure 3.3) consists of two concentric tubes ("Tube-in-Tube" heat exchanger technique) with the function of transferring the heat of a fluid from a tube to another. The internal pipe is used for the high pressure to reduce the radial stresses due to its smaller diameter.

For the heat exchanger dimensioning, there are two major concerns:

- To ensure that the pressure drops caused by the resistance to the flow do not significantly decrease the pressures along the system in order to avoid losses of performance. This is achieved with short heat exchangers or with large enough hydraulic diameters.

- To ensure that, if possible, it behaves as an ideal heat exchanger, which means that all the heat that can be exchanged is exchanged along the heat exchanger. It can be achieved by increasing the length thus increasing the contact area between the two fluids.

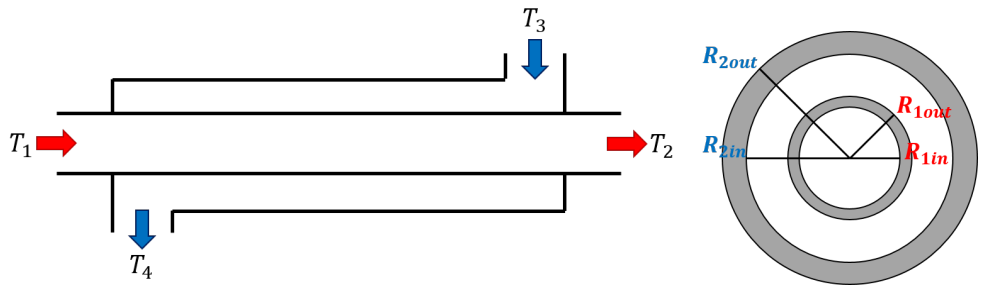

a Schematic b Radius

Figure 3.3: Counterflow heat exchanger

3.2.1 Calculation of the pressure drop in HX tubes versus diameter

The most important parameter about choosing the diameter of the tubes is the pressure drop in the tubes , ΔP, given by the expression below[6]

$$\frac{\Delta P}{L} = f_D \frac{\rho}{2} \frac{V^2}{D} \tag{3.3}$$

Where f_D is the friction factor of the fluid. This factor is very sensitive to the fluid regime (laminar or turbulent); in turbulent regime, it also depends on the roughness of the tube walls. Its variation with the Reynolds number, R_e, is depicted in the Moody diagram (figure 3.4).

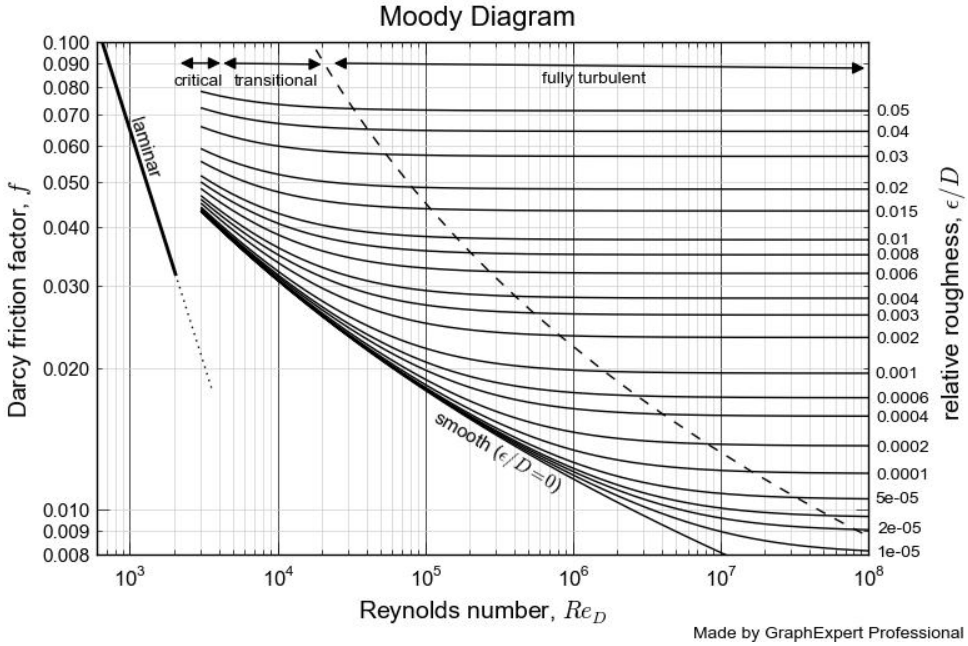

Figure 3.4: Moody diagram made by GraphExpert Professional

The Reynolds number is the ratio between the inertial forces and viscous forces and, as show in figure 3.4 allows knowing the flow regime. It depends on the kinematic viscosity of the fluid, ν, the tube hydraulic diameter, D_h, and the mean velocity of the fluid, V:

$$R_{e\ D_h} = \frac{V D_h}{\nu} \tag{3.4}$$

The kinematic viscosity of the fluid, ν, is given by the ratio between the dynamic viscosity, μ, and density, ρ,

$$\nu = \frac{\mu}{\rho} \tag{3.5}$$

And the mean velocity of the fluid, is given by the folowing expression:

$$V = \frac{\dot{V}}{A} = \frac{\dot{m}}{\rho A} \tag{3.6}$$

Being $\dot{V}$ the volumetric flow rate and A the cross section.

$$A = \frac{\pi}{4} {D_h}^2 \tag{3.7}$$

In our case, for a mass flow of 23.7 mg/s and at a temperature of 180 K (that is the worst case to ensure its working), applying these equations for both tubes, we calculate the Reynolds number as a function of the diameter (figure 3.5) in order to know the regime existing in the tubes. Note that for the low pressure tube, the hydraulic diameter is the difference between the tubes diameters.

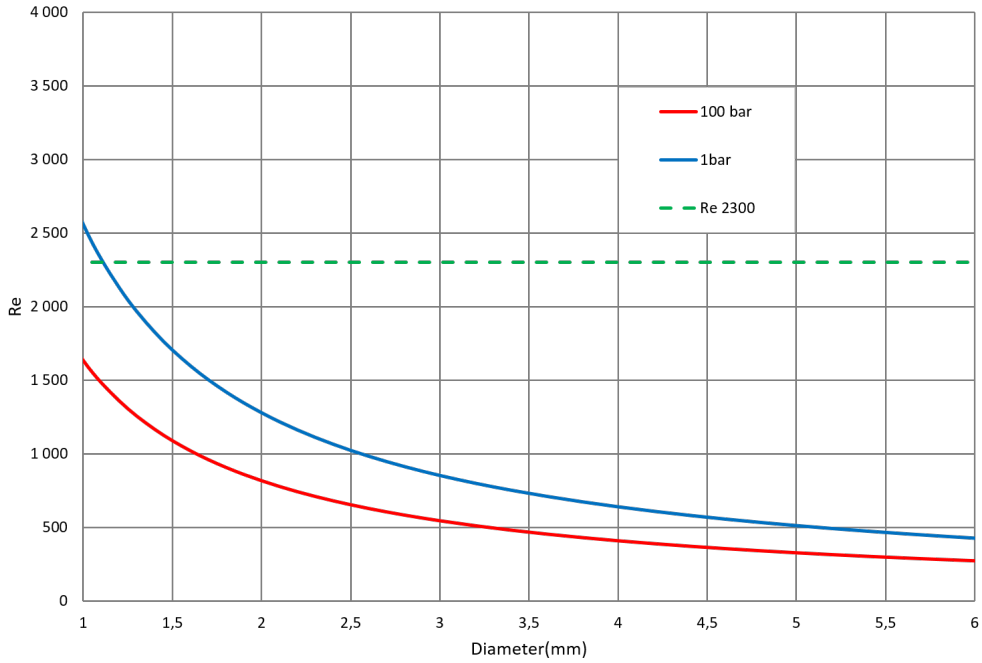

Figure 3.5: Graph of the evolution of Reynolds number with diameter

As demonstrated in figure 3.5: For high pressure, the fluid is clearly in laminar regime (R_e lower than 2300) to the different diameters, due to the high density of the fluid. For the lower pressure, to diameters lower than 1.2 mm, we are in the transition region to the turbulent regime but a priori these diameters are excluded, so it is also in laminar regime.

If the turbulent regime (R_e higher than 4000) was reached, it would be necessary to use the Colebrook–White equation to calculate the f_D but in our case, laminar flow, f_D is simpler and given by the following expression:

$$f_D = \frac{64}{R_e} \tag{3.8}$$

which leads us to the next simple analytical expression for the pressure drop,

$$\frac{\Delta P}{L} = 128\mu\frac{\dot{V}}{\pi D^4} \tag{3.9}$$

Using this expression, it is possible to trace the dependence of the pressure drop per meter as a function of the tube diameter hydraulic for high and low pressure (figure 3.6).

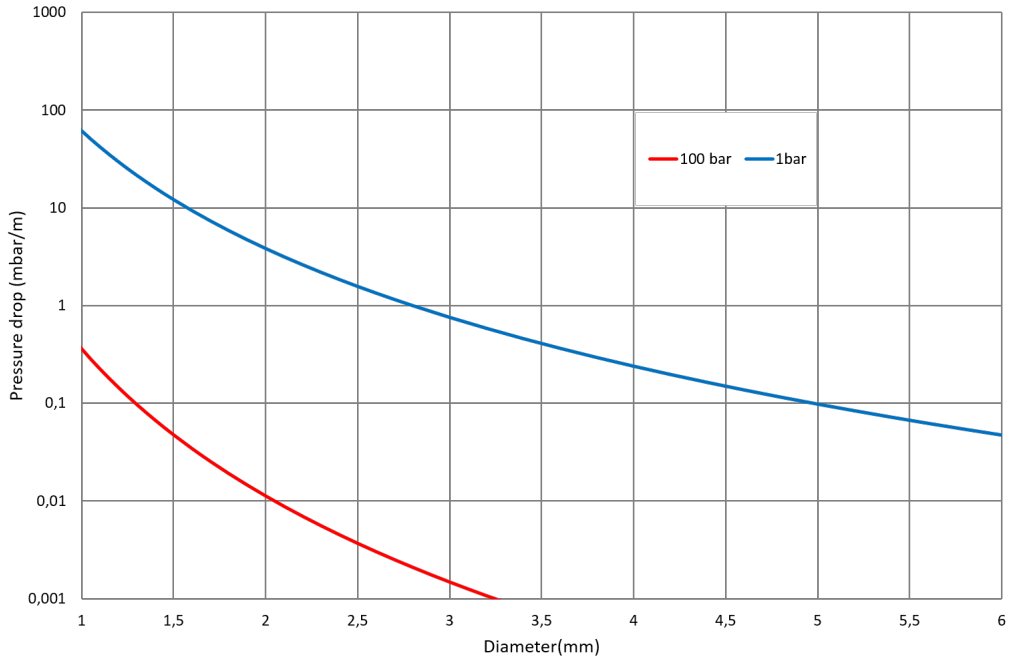

Figure 3.6: Curve of the evolution of pressure with diameter

Considering a pressure drop lower than 1 mbar/m for both sides, that is not too disturbing for the performance of the system, it can be seen that beyond 1 mm of diameter in high pressure tube, and 2.8 *mm* of diameter in lower pressure tube, the pressure drop is quite insignificant.

3.2.2 Calculation of the tube thickness

It is now necessary to calculate the required thickness of the tubes to hold the pressure. In the case of capillaries, the name given to small diameter tubes, we can use the thin walls approach, applicable when the wall thickness is less than about a tenth of its radius[7].

In this case, it is only necessary to consider the radial stress and the following expression allows to calculate the thickness.

$$\sigma = \frac{rP}{t} \tag{3.10}$$

The thickness, t, is dependent on the yield strength of the material of the pipe walls, σ, on his radius, r and on the subject pressure, P. To determine the thickness, it is only considered the high pressure side because it is the most critical, with a pressure of 100 bars. The wall material is composed by 304 stainless steel that has a yield strength of 250 MPa.

Using the approach for thin walls, we plot the thickness in function of the inner diameter of the high pressure tube (figure 3.7).

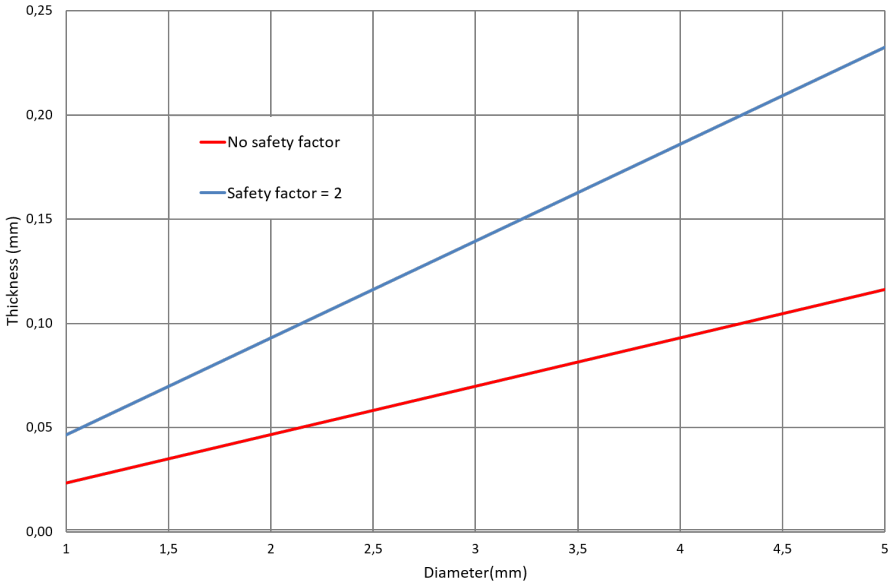

Figure 3.7: Thickness of the high pressure tube vs the inner diameter

As a precaution, it was set a thickness of $0.25mm$ because it is admissible for any diameter and it has a safety factor greater than 2.

In order to confirm the veracity of this approach there is the K factor, which is given by the ratio between the diameter and the thickness.

$$K = \frac{D}{t} \tag{3.11}$$

To these thickness, the K factor is 43, which indicates an error to the approach lower than 1% (figure 3.8).

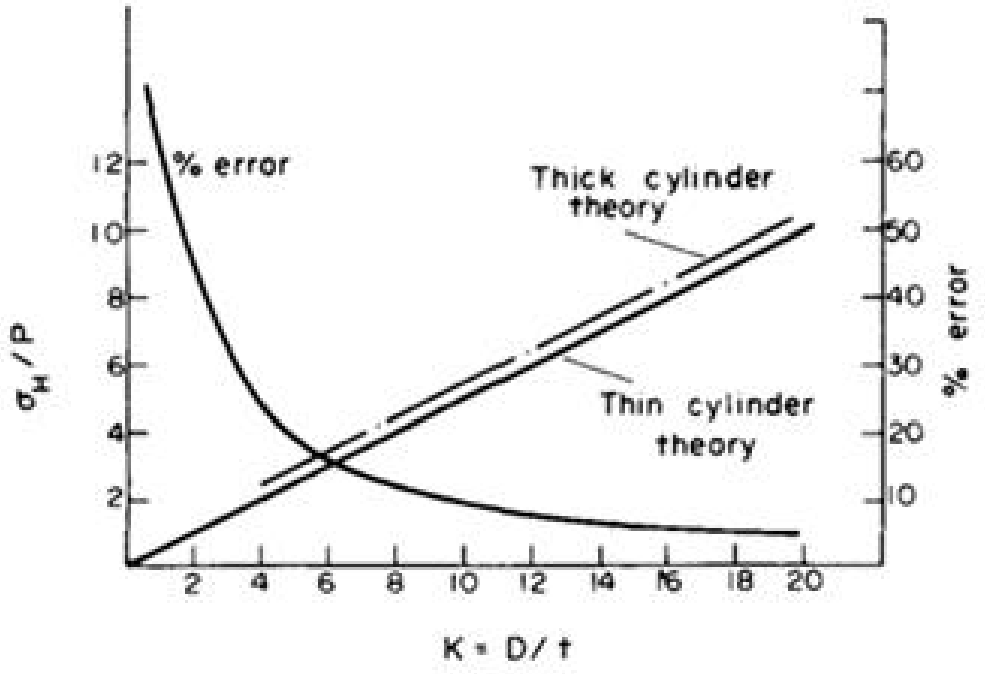

Figure 3.8: Comparison of thin and thick cylinder theories for various diameter/thickness ratios[8]

3.2.3 Thermal exchange in the HX versus length

Knowing the diameters and the thickness of the tubes, the last geometrical parameter to take into account for efficiency of the heat exchanger is its length. Applying the equations of heat balance at any point of the exchanger for an isolated system and using the notation defined in the figure 3.3a, temperatures T_2 and T_4 are given by the equations[9],

$$(T_1 - T_2) = \eta(T_1 - T_3) \tag{3.12}$$

$$(T_4 - T_3) = \frac{W_{12}}{W_{34}}\eta(T_1 - T_3) \tag{3.13}$$

being,

$$W = \dot{m}c_p \tag{3.14}$$

The efficiency of the exchanger, η , which depends on the fluid, the diameter of the inner tube (D) and the length (L) is given by:

$$\eta = \frac{1 - e^{-\alpha}}{1 - \frac{W_{12}}{W_{34}}e^{-\alpha}} \tag{3.15}$$

$$\alpha = \left(\frac{1}{W_{12}} - \frac{1}{W_{34}}\right)h_0\pi DL \tag{3.16}$$

To help to understand the operation of the counterflow heat exchanger and the equations it is represented in figure 3.9 an example for the case where $c_{p\ hot} > c_{p\ cold}$.

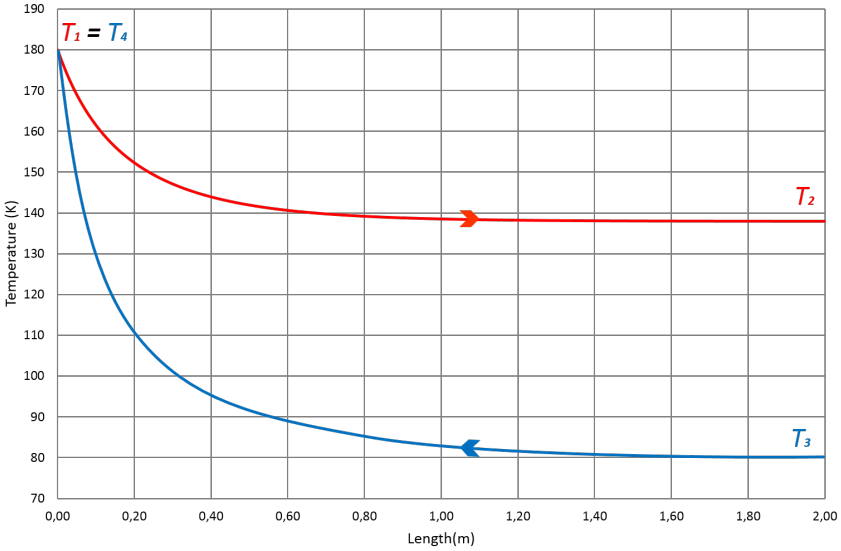

Figure 3.9: The temperatures profile inside the heat exchanger using notation of figure 3.3

In this last expression, h_0 is the overall heat transfer coefficient of the heat exchanger. It depends on the heat transfer coefficient of the fluid in the hot and cold side, h_{in} and h_{out}, on the conductivity of the material that separates the two tubes, k, and on the radius of the heat exchanger tubes (figure 3.3b)[9]. It can be demonstrated

$$\frac{1}{h_0} = \frac{r_{1out}}{h_{in} r_{1in}} + \frac{r_{1out}}{k} \ln\left(\frac{r_{1out}}{r_{1in}}\right) + \frac{1}{h_{out}} \tag{3.17}$$

Finally it is necessary to calculate the heat transfer coefficient for fluids, h_{in} and h_{out}. In the case of a forced convection inside tubes it can assume the following expression

$$h = \frac{N_u k}{D} \tag{3.18}$$

Being the Nusselt number, N_u the ratio between the heat transferred by convection and conduction:

$$\mathrm{Nu}_L = \frac{\text{Total heat transfer}}{\text{Conductive heat transfer}} = \frac{hL}{k} \tag{3.19}$$

In our case, as we are in laminar flow and we have an uniform surface heat flux for circular cross section tubes, the Nusselt number is constant[6],

$$N_u = 4.36 \tag{3.20}$$

For technical reason, an outside diameter of 5.4 mm was the most appropriate for the low pressure tube. Using this value: the output temperature of the high-pressure pipe, T_2, vs L for various inner diameter of the high pressure tube was plotted (figure 3.10).

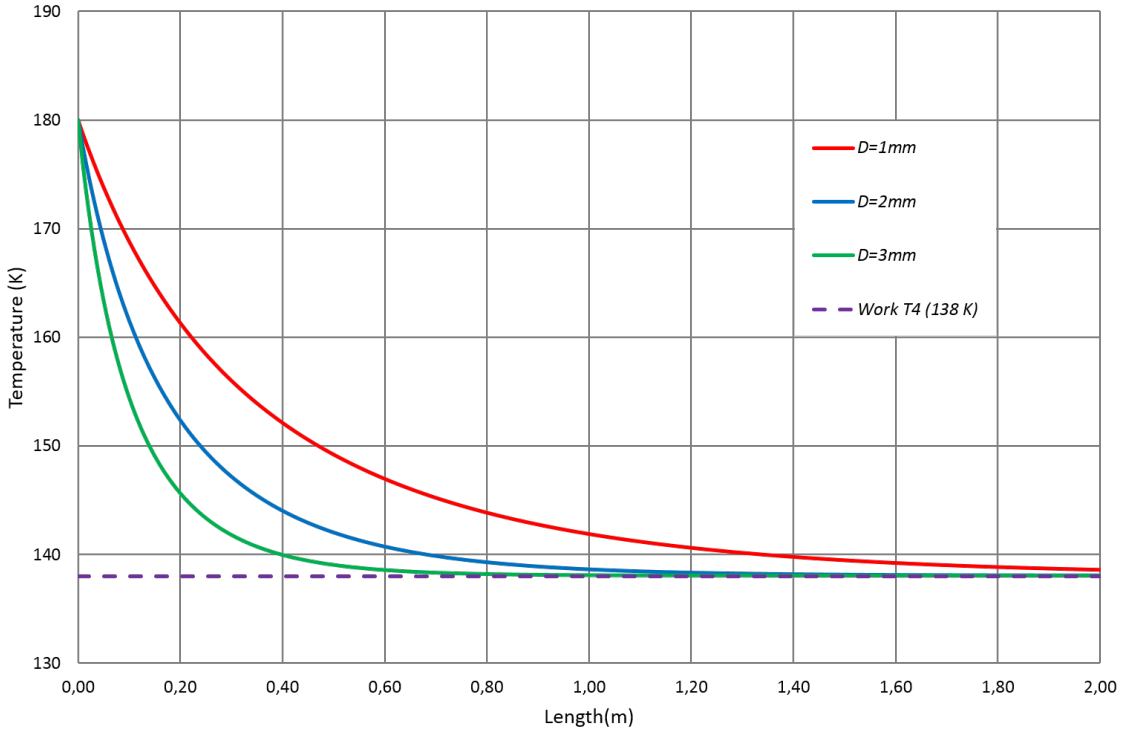

Figure 3.10: Plot of the output temperature of the high-pressure pipe with the length in the heat exchanger.

If we want to exclude HX longer than 2 meters, based on the plot we can exclude the diameter of 1 mm because it is not enough to cool the fluid to the desired temperature (138 K). In opposition the diameters of 2 mm and 3 mm are long enough to achieve the desired temperature.

Now, to choose between tubes it is necessary to confirm if the pressure drops are not significant. Remember that for the high pressure tube, the diameter had to be higher than 1 mm and for the low pressure tube, had to be higher than 2.8 mm.

Both diameters of the high pressure tube are higher than 1 mm, so we could chose any one. However, when we calculate their hydraulic diameters, not forgeting of adding their thickness, to the low pressure tube, we obtain an hydraulic diameter of 2.9 mm with the tube of 2 mm and 1.9 mm for the of 3 mm. Therefore, the tube of 3 mm is excluded and the chosen one is the tube of 2 mm.

With the chosen diameters we can plot the temperature profile along the length of the heat exchanger tubes (T_2 and T_4) to define the length of heat exchanger. Those temperatures are represented in the next graph (figure 3.11). From this plot (figure 3.11), it can be seen that in exchangers with a length, L, longer than ≈1.5 m, T_2 and T_4 do not change significantly any more which indicates that the ideal would be to construct a heat exchanger with 2 m. In this way it is ensured that all the heat is exchanged between the sides with a efficiency, η, of 41.99% (maximum 42%) and a performance of 99.99%.

Also, it is important to note that the fact that there is a larger temperature variation on the cold side in relation to the hot side that allows the T_4 temperature to be equal to T_1 is due to the fact that the heat capacity of nitrogen at a constant pressure of 100 bars is higher than at 1 bar.

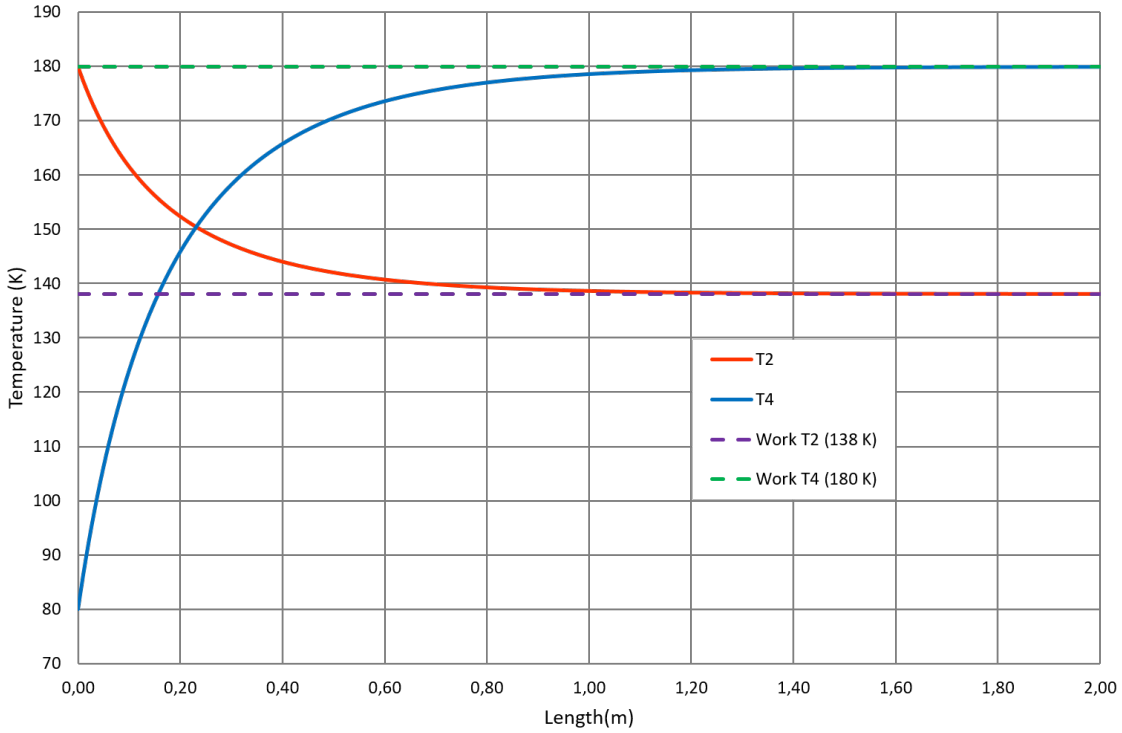

Figure 3.11: Plot of temperature evolution with the length of the heat exchanger

To sum up the heat exchanger dimensions are displayed in table 3.2.

Table 3.2: Heat exchanger dimensions

D_{1in}	2 mm
D_{1out}	2.5 mm
D_{2in}	5.4 mm
D_{2out}	6 mm
L	2 m

3.3 Joule-Thomson valve

A Joule-Thomson valve expansion consists on forcing the gas to pass through a restriction, small enough to cause a significant pressure drop (isenthalpic expansion).

The way of characterizing the Joule-Thomson valve effect is through the Joule-Thomson coefficient,

$$\mu_{JT} = \left(\frac{\partial T}{\partial P}\right)_H \tag{3.21}$$

The Joule-Thomson coefficient indicates if the temperature increases or decreases after an expansion ($dP < 0$). From equation 3.21, we can see that the fluid inversion temperature corresponds to the temperatures for which this coefficient is equal to zero and the fluid cools only if $T_{in} < T_{inv}$. The red curve limits the zone where the temperature decreases after the expansion to a certain pressure (figure 3.12).

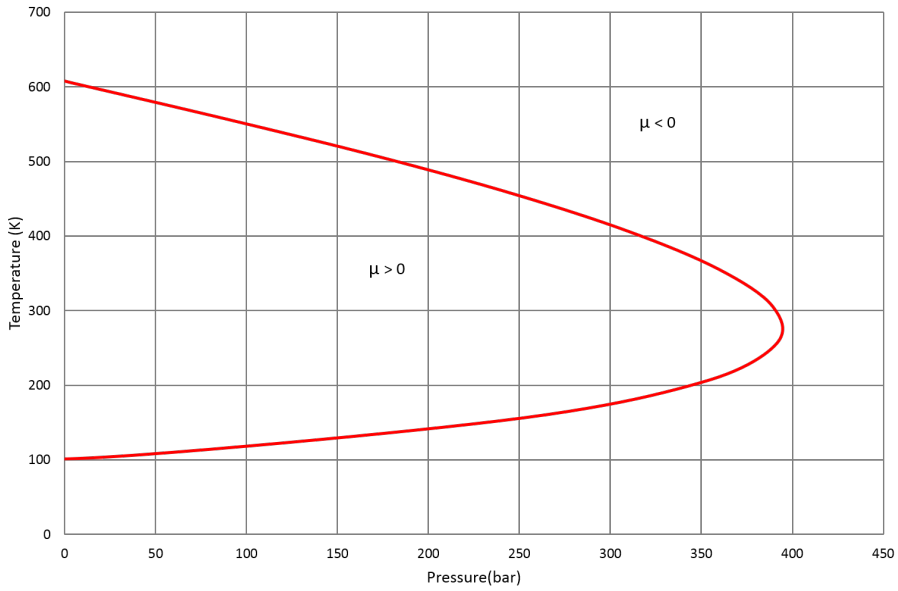

Figure 3.12: Graph of nitrogen inversion curve on the Joule-Thomson limits the zone of decreasing temperature

The valves that we tested were basically constituted by a gland with a hole in its center, this hole was made with a laser beam. The diameter of this hole must ensure the target mass flow of nitrogen at the pressure and temperature wanted.

When a compressible flow finds a restriction, by the principle of mass conservation, the velocity needs to increase to cross the restriction (figure 3.13). The fluid speeds up until it reaches the sound velocity of this fluid under such conditions of pressure and temperature. This effect is called choked flow, the velocity of the fluid becomes choked or limited, and it is an isentropic process. But this is just local a process, after that the gas is forced to lower its temperature due to the pressure drop at a constant enthalpy[10].

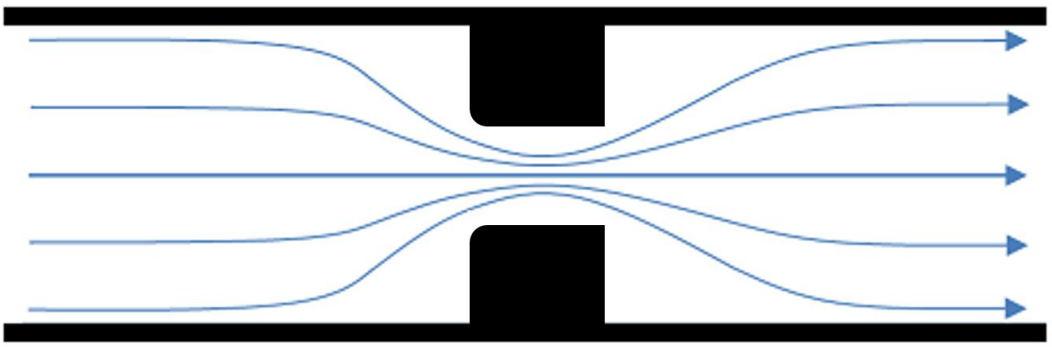

Figure 3.13: Schematic of the Joule-Thomson valve

In choked conditions and assuming an ideal gas behaviour, the equation for the mass flow rate in SI units is:

$$\dot{m} = C_d A \sqrt{k\rho P \left(\frac{2}{k+1}\right)^{\frac{k+1}{k-1}}} \tag{3.22}$$

Being C_d the discharge coefficient (ratio of the actual discharge to the theoretical discharge), A the restriction cross-sectional area, k the heat capacity ratio (C_p/C_v), ρ the density before expansion and P the upstream pressure.

Actually, the problem is not simple. For instance, in our working conditions (100 bar and 138 K), the fluid can not be considered an ideal gas. To overcome this problem we have two main ways: one is to use real gas property data, like those given by REFPROP program [11], and the discrepancy in respect to these results incorporated in a C_d;

The other way is to use the correlations from a model developed by Maytal et al., also to ideal gas[12]. So, considering the density of an ideal gas,

$$\rho = \frac{P}{TR_s} \tag{3.23}$$

Being R_s the specific gas constante (in case of nitrogen $R_s = 296.8 J/kg.K$), it is possible to rewrite the mass flow expression for an ideal gas.

$$\dot{m}_{ideal} = C_d A P \sqrt{\frac{k}{TR_s}\left(\frac{2}{k+1}\right)^{\frac{k+1}{k-1}}} \tag{3.24}$$

In the Maytal's model, the isentropic and isenthaplic conservation law through the process is solved considering that the flow velocity at the end of the expansion is equal to the sound velocity. Considering the law of the corresponding state, a correlation factor, Γ, is obtained as a function of the reduced pressure ($\Pi_0 = P/P_c$), and temperature ($\Theta_0 = T/T_C$). For instance, these correlations for nitrogen are given in figure 3.14.

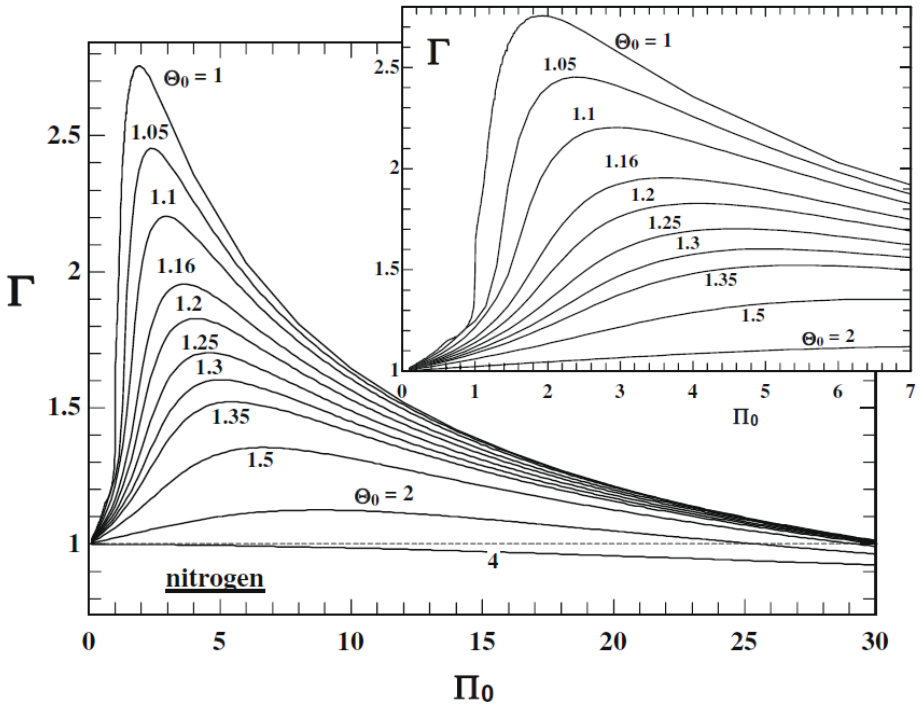

Figure 3.14: The Maytal correlation factor[12]

Then for real gases it is applied the correlation factor (Γ)

$$\dot{m} = \Gamma \dot{m}_{ideal} \tag{3.25}$$

The restrictions available had a diameter of 25 μm and 45 μm so we had to use them to test the veracity of these correlations in order to size the right diameter giving the right flow (23.7 mg/s) at the right pressure (100 bar) and the right temperature (138 K).

Chapter 4

Experimental Setup

During the course of the thesis, it was decided to test the Joule-Thomson (JT) valve separately of the counterflow heat exchanger. This decision was driven by the necessity to characterize the JT orifices in real conditions of pressure and temperature, independently of the performances on counterflow heat exchanger. Such strategy would theoretically help to detect the cause of an eventual dysfunction of the cold part.

4.1 Experimental setup for the Joule-Thomson valve

To characterize the JT valve it was necessary the to design a system capable to create the real conditions (T_{in} and P_{in}) at the input of the JT restriction. This system was divided in two parts: one responsible for the pressure and mass flow (gas bottle, pressure regulator and manifold) and other for the temperatures (Cold finger). The schematic of the system used is represented in figure 4.1.

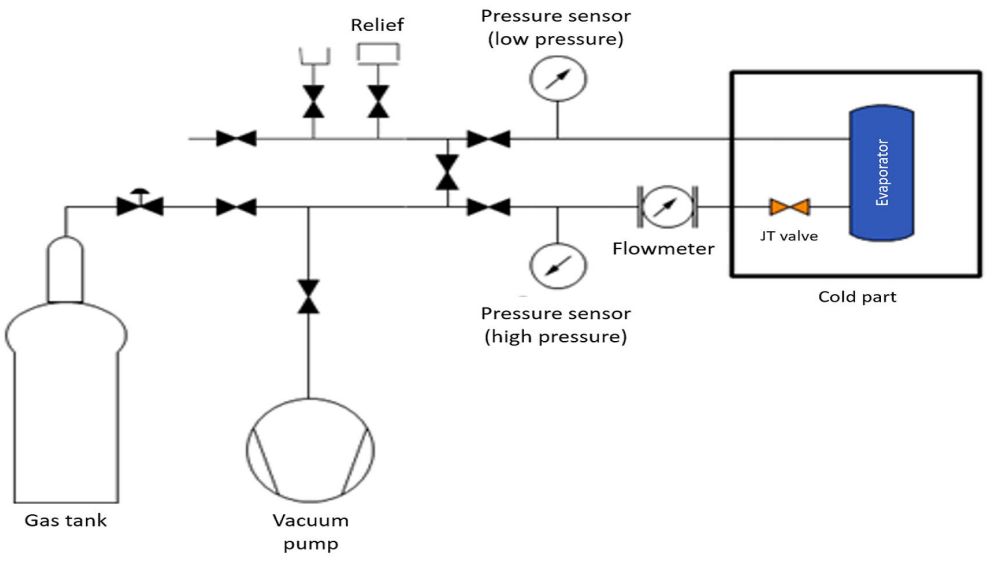

Figure 4.1: Schematic of the system used

In this early stage of this project, the sorption compressor, responsible for providing a gas flow, was still under study and was substituted by a pressurized gas bottle equipped with a pressure regulator. This gas bottle ("B50" cylinder) provides and maintains the necessary gas flow to the system and then the gas is released to atmosphere by a home-made one way valve. Actually, this system was very functionnal for the tests performed during this work due to its low costs and simplicity.

The valve panel (manifold) built is showed in figure 4.2 as well as the gas bottle and pressure regulator. Let us note that this panel was designed by Jorge Barreto in order to incorporate others funcionalities allowing to work with neon in the next future. This panel has the function of managing the course of the fluid and to measure the pressure and mass flow.

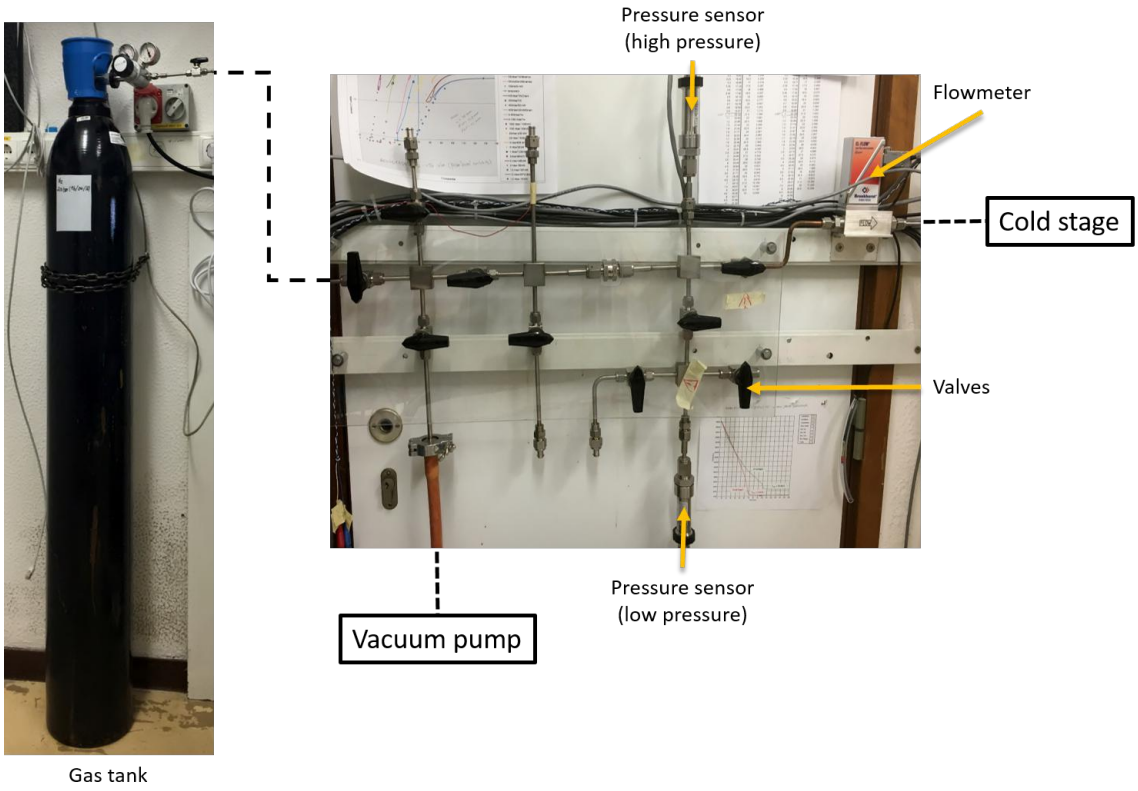

Figure 4.2: Gas control system assembly

To provide the right temperature (138 K) at the input of the JT valve was not so easy, to do this it was necessary to use a cryocooler already existing in the Cryogenic lab. The cryocooler was adapted like demonstrated in the next figure 4.3.

This part of the system is constituted by two heat exchangers (HX1 and HX2) that allow us to control the temperature at which occurs the expansion in the Joule-Thomson valve, with the help of the cryocooler. Those heat exchangers are essentially a tube in which flows the nitrogen soldered to a copper block, this one being thermally coupled to one stage of the cryocooler.

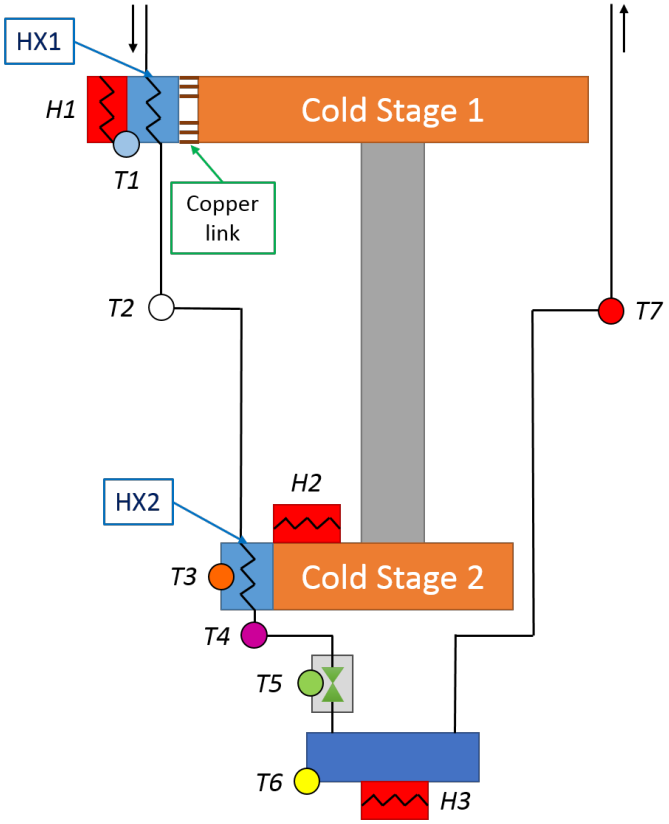

Figure 4.3: Schematic of the Joule-Thomson system

The first exchanger is thermalized in the first stage of the cryoccoler (T= 26 K, not controllable) and is responsible for precooling the gas from room temperature down to around 160 K. The final precooling down to the desired temperature (138K) is ensured by the second heat exchanger thermalized in the second stage (Cold finger). As a matter of fact, this second stage is equipped with a heater (H2) that allows to control its temperature so we attached the second heat exchanger directly to this stage and in this way we can control the different temperatures of the test by changing the temperature of the second stage.

But for this to work it was necessary to calculate the correct dimensions of the heat exchangers that enable to simulate normal work conditions, 100 bar and 138 K at the entrance of the Joule-Thomson valve with a mass flow of 23.7 mg/s.

Using the same type of calculation that was used in section 3.2.3, it is obtained the following expression for the length [9]:

$$(T_0 - T_2) = (T_0 - T_1)e^{-\frac{\pi hDL}{\dot{m}c_p}} \tag{4.1}$$

being T_0 the temperature of the copper block, T_1 the temperature of the fluid at the heat exchanger inlet and T_2 the outlet.

Using the previous expression for HX1 it is possible to trace the evolution of the temperatures as a function of the length of the heat exchanger. This is demonstrated in

the next plot (figure 4.4), where we can see that after 65 mm the temperature of the gas temperature decreased from room temperature down to 160 K which is low enough to allow a second heat exchanger relatively short do the rest.

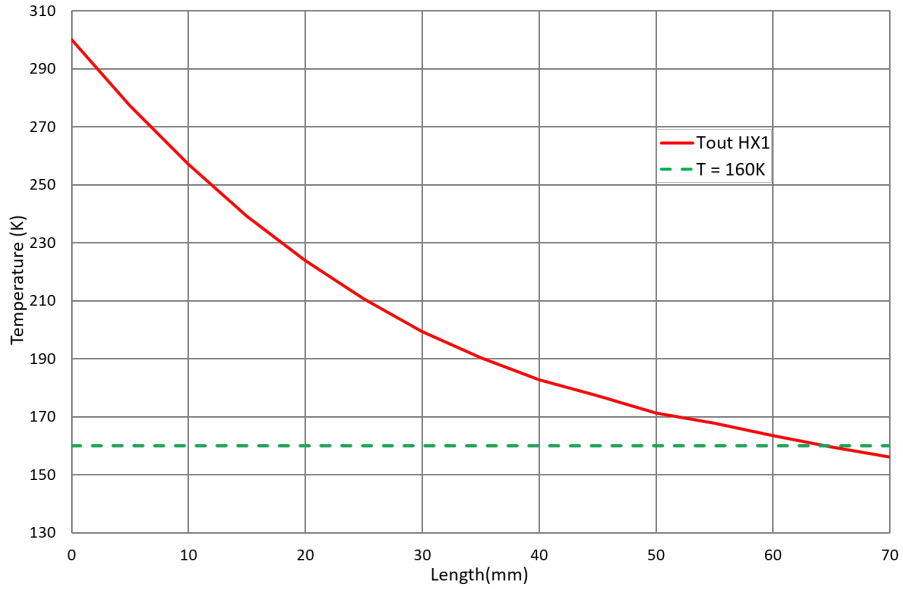

Figure 4.4: Plot of the evolution of the temperatures with the length in HX1

Again using the previous expression for HX2 we can calculate the evolution of the temperatures with the length of the heat exchanger. In figure 4.5, it can be seen that using a temperature of 50 K in the second stage and 20 mm long heat exchanger it is possible to achieve temperatures around 138 K, that is the same temperature that we want to achieve at the outlet of the conyterflow HX (see section 3.1).

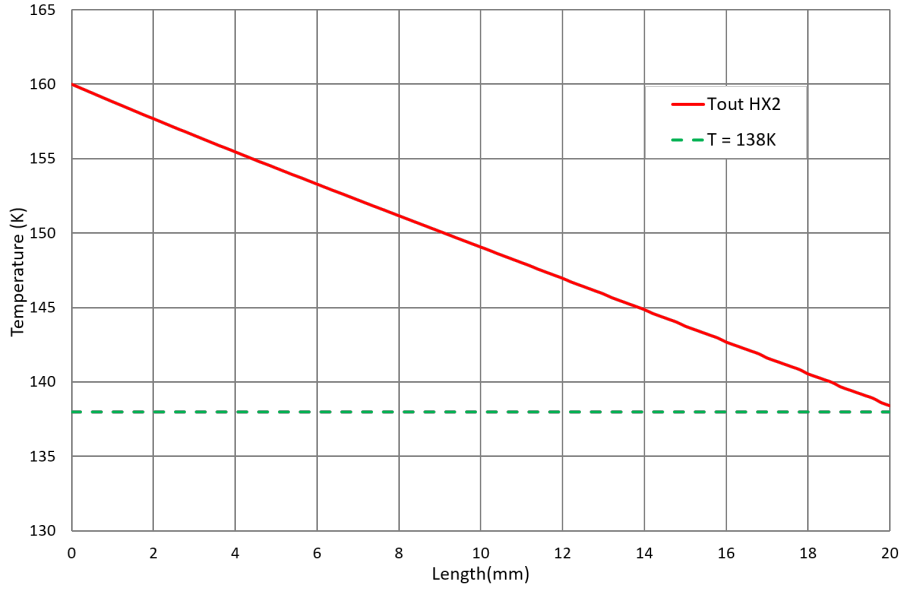

Figure 4.5: Plot of the evolution of the temperatures with the length in HX2

Actually, we faced the following technical problem: if we connect the first heat exchanger directly in the first stage, it will cool down to a temperature between 25-30K, equilibrium temperature of this stage, not controllable, then, at the beginning of an experiment, when the nitrogen starts to circulate, it solidifies ($T_{sol} \approx 63K$), clogging the tube along this HX without any solution to restore the nitrogen flow. To solve this problem, we limited the power exchanged between the HX1 and the first stage by using a copper link and installing a heater resistor, H1, (300 Ohms) on the HX1 copper block . The copper link allows cooling the heat exchanger but also to warm it with a reasonable heating power when necessary.

To dimension this copper link, taking into account that it must allow a gas cooling down to at least 160 K in the stationary regime (constant mass flow), we considered that the cooling power at 160 K needed to cool the gas from room temperature (equation 4.2) is provided by this heat link (equation 4.3), with $\Delta T = (160K - 25K)$ and a mass flow a little higher, around 35 mg/s in order to consider a possible higher mass flow that could occur due to uncertainty in the JT performances.

$$\dot{Q} = \dot{m}(H_{300K,100bar} - H_{160K,100bar}) \tag{4.2}$$

$$\dot{Q} = -k\frac{S}{L}\Delta T \tag{4.3}$$

This calculation indicates that 6 wires of copper (RRR= 100), with 60 mm long and 1 mm of diameter, mounted in parallel would be a good solution.

In the system it was also set several thermometers with the function of registering the temperature along the circuit (see figure 4.3). After the JT valve, a third heater (H3) was solded on the tube that allowed to evaporate the liquid nitrogen in case of its formation with a power maximum of 2 W.

4.1.1 Manufacturing of the Joule-Thomson system

The first heat exchanger (HX1)

The first heat exchanger consists on a tube (65 mm long and 1.5 mm inner diameter) wrapped around a copper cylinder with a diameter of 12 mm. Being this diameter relatively small, we had to prevent some tube crushing during this winding: the tube was first filled with liquid water, freezed, and then wound around the copper cylinder. After the shaping phase, the tube was then welded with a soft solder ($Sn_{96.3\%}Ag_{3.7\%}$) with a melting point of $221°C$ (figure 4.6a).

The copper link was made using 6 wires welded to a plate of copper. After that the HX1 was assembled in the cryocooler as shown in figure 4.6b.

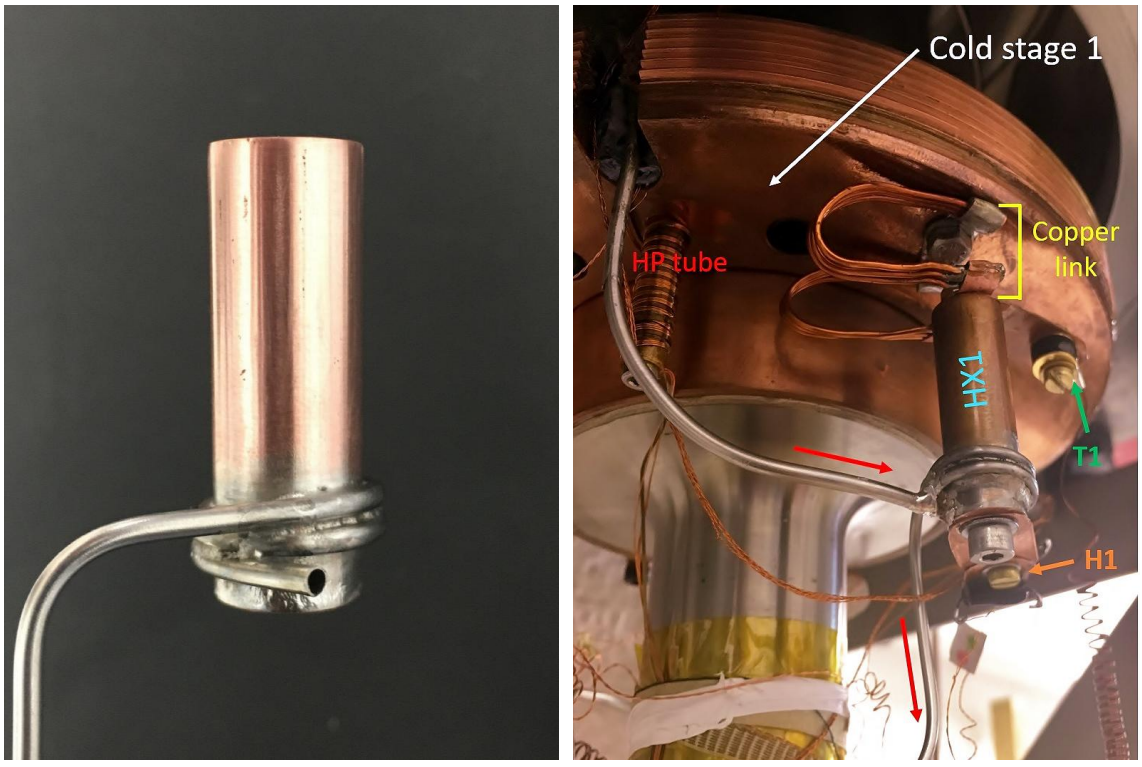

a HX1 b HX1 coupled to 30 K stage

Figure 4.6: The first heat exchanger (HX1)

The second heat exchanger (HX2)

For this HX2, only 20 mm long, the tube was welded on a copper foil directly connected to the second state of the cryocooler (Figure 4.7a).

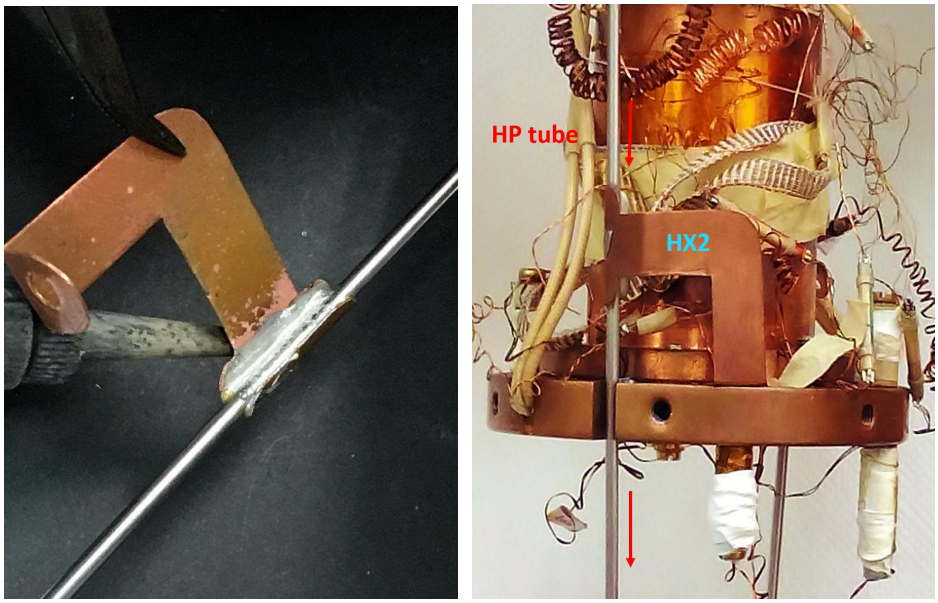

a HX2 b HX2 assembled on cold finger stage

Figure 4.7: The second heat exchanger (HX2)

Joule-Thomson valve

The Joule-Thomson valve was manufactured from a Swagelok©VCR Blind Gland of 1/4 inch. First, the Gland was drilled with a diameter of 4.75 mm to obtain a thickness of 2.54 mm and then using a laser it was made the restriction (see in Appendix A.1.2). Being the manufacturing uncertainty of 10 %, the diameters was measured using a Scanning electron microscope, SEM, (Figure 4.8). For the orifices used in this work, diameter of 25.05 μm and 49.25 μm were mesured for nominal diameters of 25 μm and 45 μm.

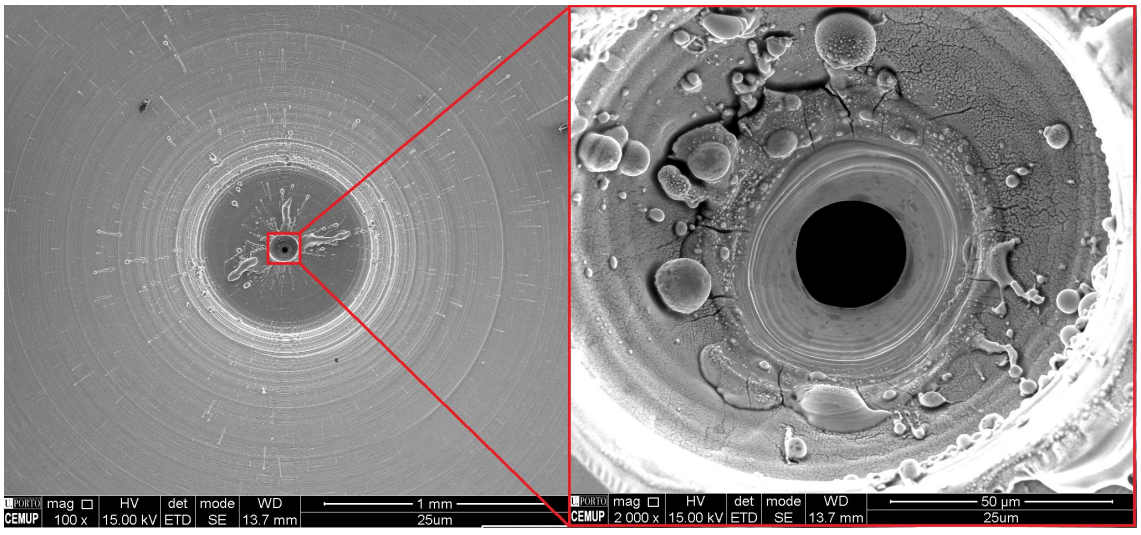

Figure 4.8: Images of the 25.05 μm restriction with SEM from Centro de Materiais da Universidade do Porto (CEMUP)

We decided to make the Joule-Thomson valve in a Blind Gland to change it more easily. To insert the gland in the gas circuit we had to manufacture others pieces to connect with the tubes, welded by the normal method.

To finish we placed the heaters and the thermometers. For both the method used was the same, a copper foil was welded directly on the tube and the heaters or thermometers were connected on the foil. All this is demonstrated on figure 4.9 and 4.10.

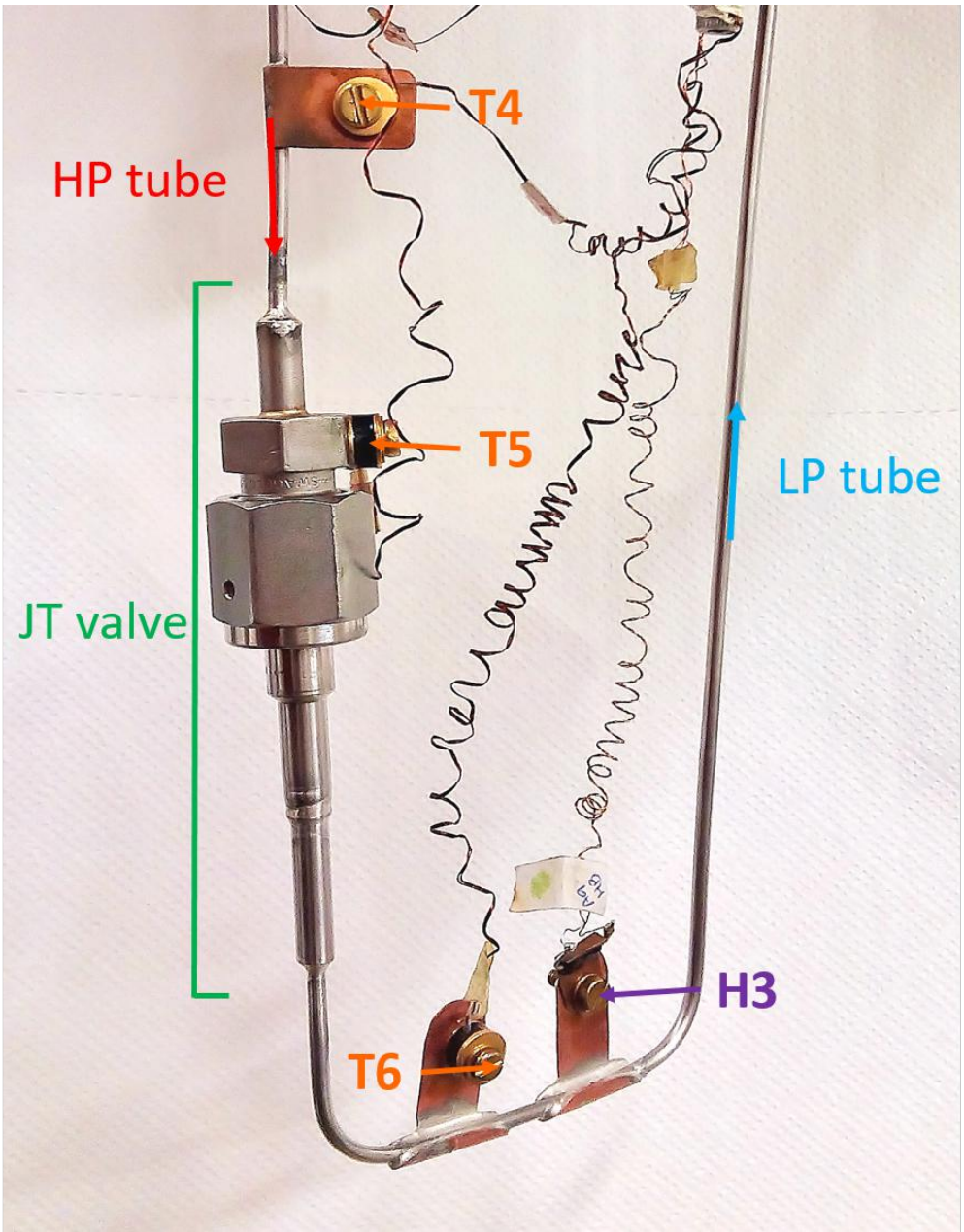

Figure 4.9: The JT valve assembly

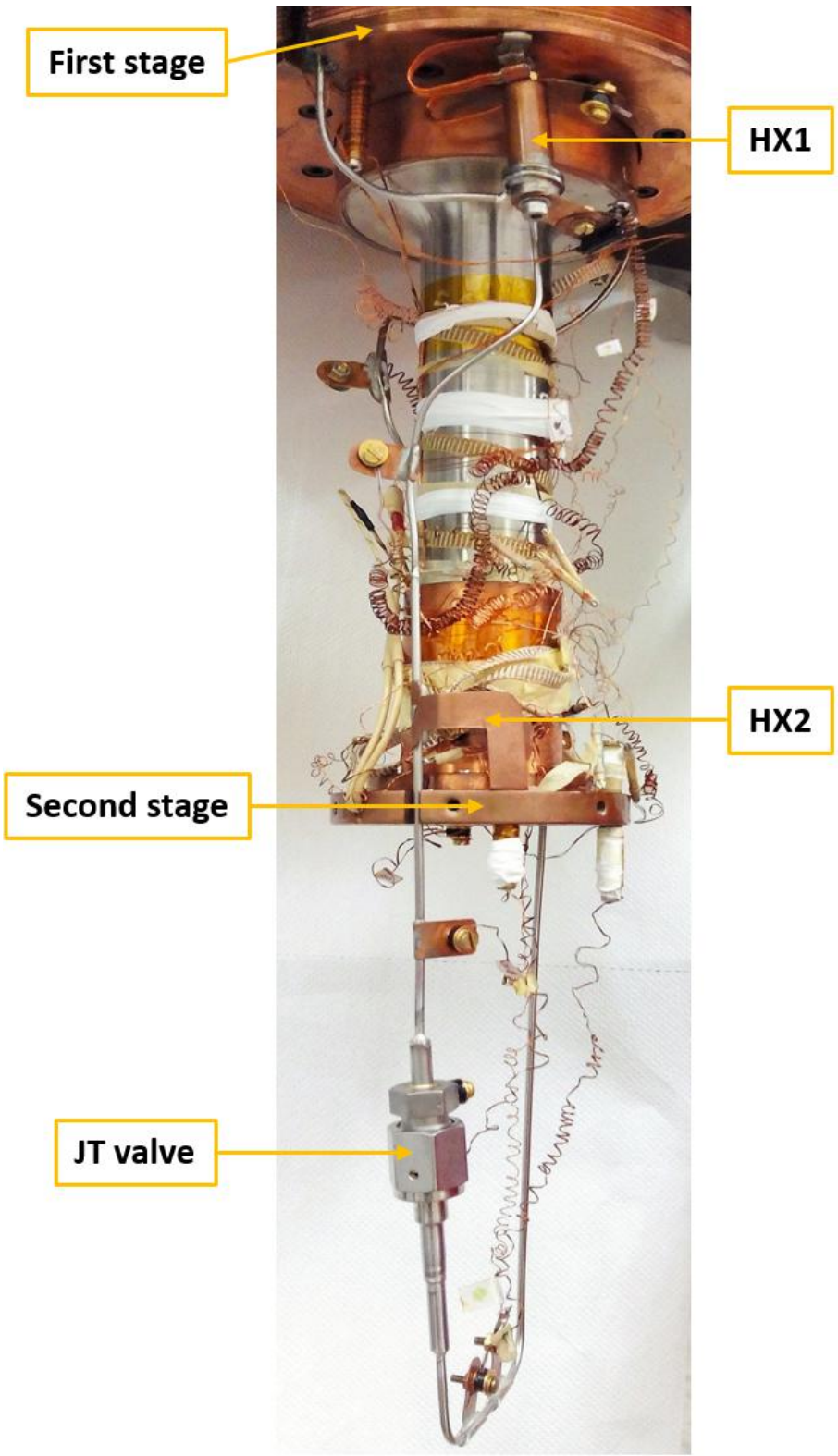

Figure 4.10: The Joule-Thomson valve overall system

4.1.2 Control and Acquisition System

The control and acquisition system uses several devices, some are indicated in figure 4.11 and others, like the Flowmeter, were already mentioned at the beginning of this chapter. The functions of the devices are described in table 4.1.

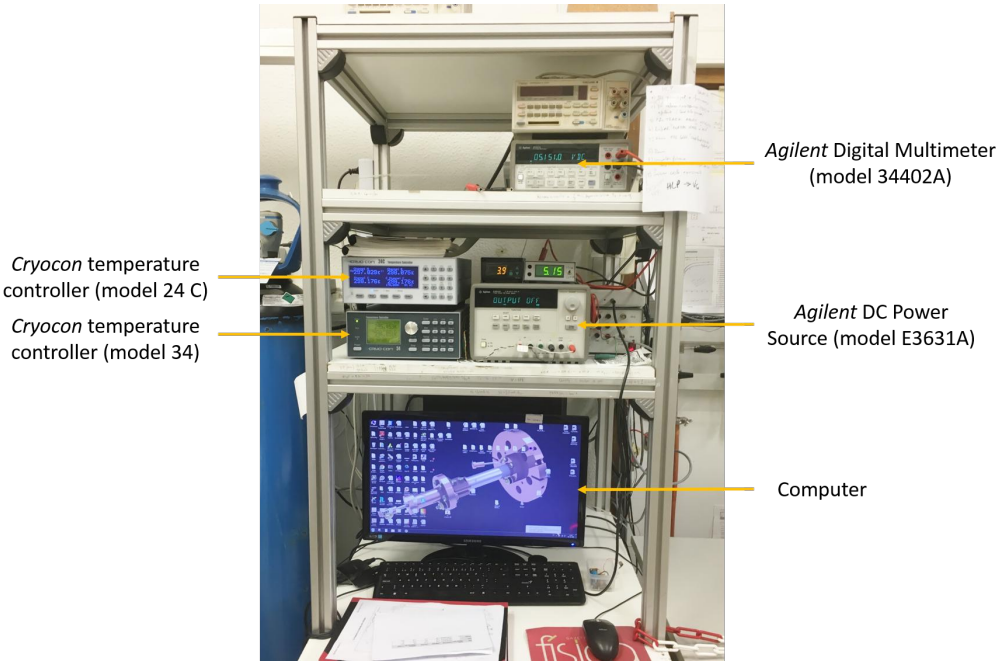

Figure 4.11: Control and Acquisition devices

Table 4.1: Functions of the control and acquisition devices

Device	Function
Cryocon temperature controller (model 24 C)	Measures several temperatures (T_1, T_2, T_7) and controls the temperature of HX1
Cryocon temperature controller (model 34)	Measures several temperatures (T_3, T_4, T_5, T_6) and controls the cold stage 2 of the cryocooler
Agilent DC Power Source (model E3631A)	Controls the Power applied (H_3) in evaporator
Agilent Digital Multimeter (model 34402A)	Measures the pressures by converting the analog signal of the pressure sensor
Computer	Communication between the $LabVIEW^{TM}$ and the devices

The interface between the devices and the user was adapted from a prior $LabVIEW^{TM}$ program that was written for this cryocooler. The program allows to measure the temperature, pressure and mass flows of the system and allows yet control temperatures and applied powers. All the parameters are recorded and saved in a data file $MicrosoftExcel^{TM}$.

The figure 4.12 displays the main interface of the $LabVIEW^{TM}$ programm. Various others "tabs" allow the monitoring of others parameters with special details.

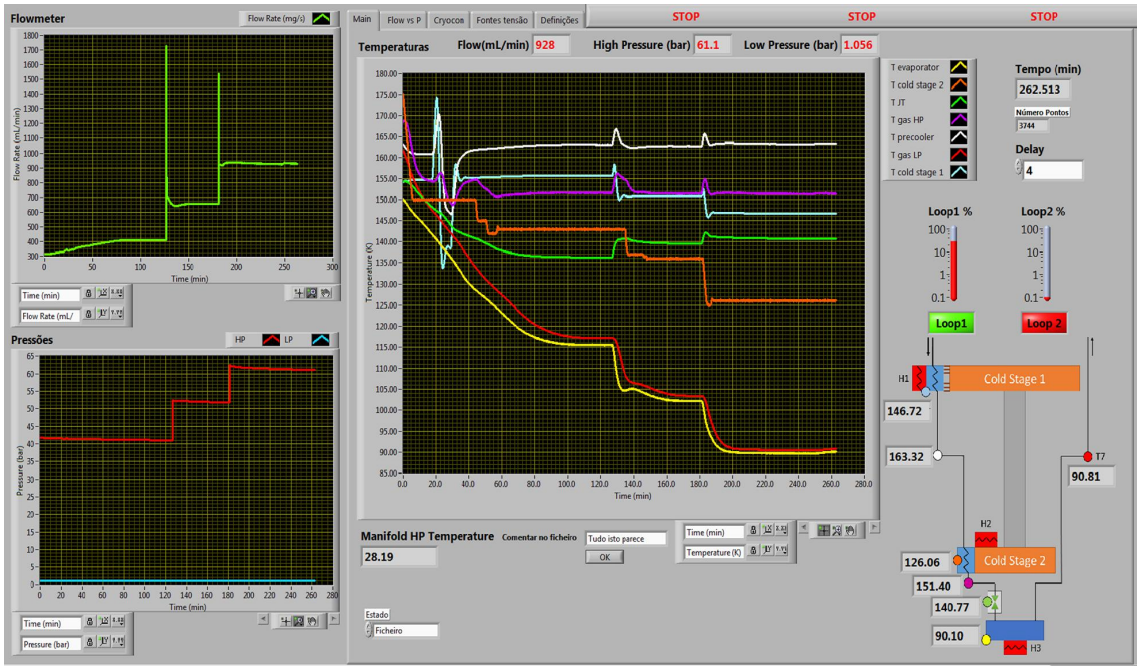

Figure 4.12: Main tab of the $LabVIEW^{TM}$ program. This tab monitors the temperature, pressure and flow rate through the system.

4.1.3 Mechanical tests

Before any test, all the pieces of the systems had to be cleaned and validated. To clean the pieces, a system made with a water pump and an ultrasound bath was mounted. The water pump was used to force the circulation of isopropyl alcohol inside the pieces, removing dirt and grease and also to make sure that nothing was clogged. Meanwhile, the piece was dipped in an ultrasound machine at $40°C$ to increase the efficiency of the cleaning process.

When required, after cleaning, all the pieces were subject to leak test with a INFICON®(model: UL1000) helium leak detector. The tests were made in vacuum mode or/and by "sniffer mode", this one allows to put the various tubes under pressure, namely closer of the real conditions. All of the pieces must had a gas leak inferior to $\approx 10^{-7}$ mbar.L/s.

After these leak tests, it was made a pressure test on the pieces. They were subjected to a pressure a little higher than the work pressure, to see if the pieces and welds sustain the working pressure. To finish, was made another leak test to make sure that no leak appeared due to the pressure test.

4.2 Experimental setup for the Cold part

Without the correct Joule-Thomson restriction we could not test the entire cold stage and consequently the counterflow heat exchanger, because we do not have the right mass flow in the right conditions. It was decided that in first place we would project the cold stage in SOLIDWORKS without the JT valve. Because the entire low temperature part will be tested in a small cryocooler (2W@ 20K) available in the Cryogenics lab, it was necessary to take into account the dimmensions already defined by this cryocooler. And this way, we could ensure that everything fits before assembling and also helped the dimensioning of others pieces. The result is showed in figure 4.13.

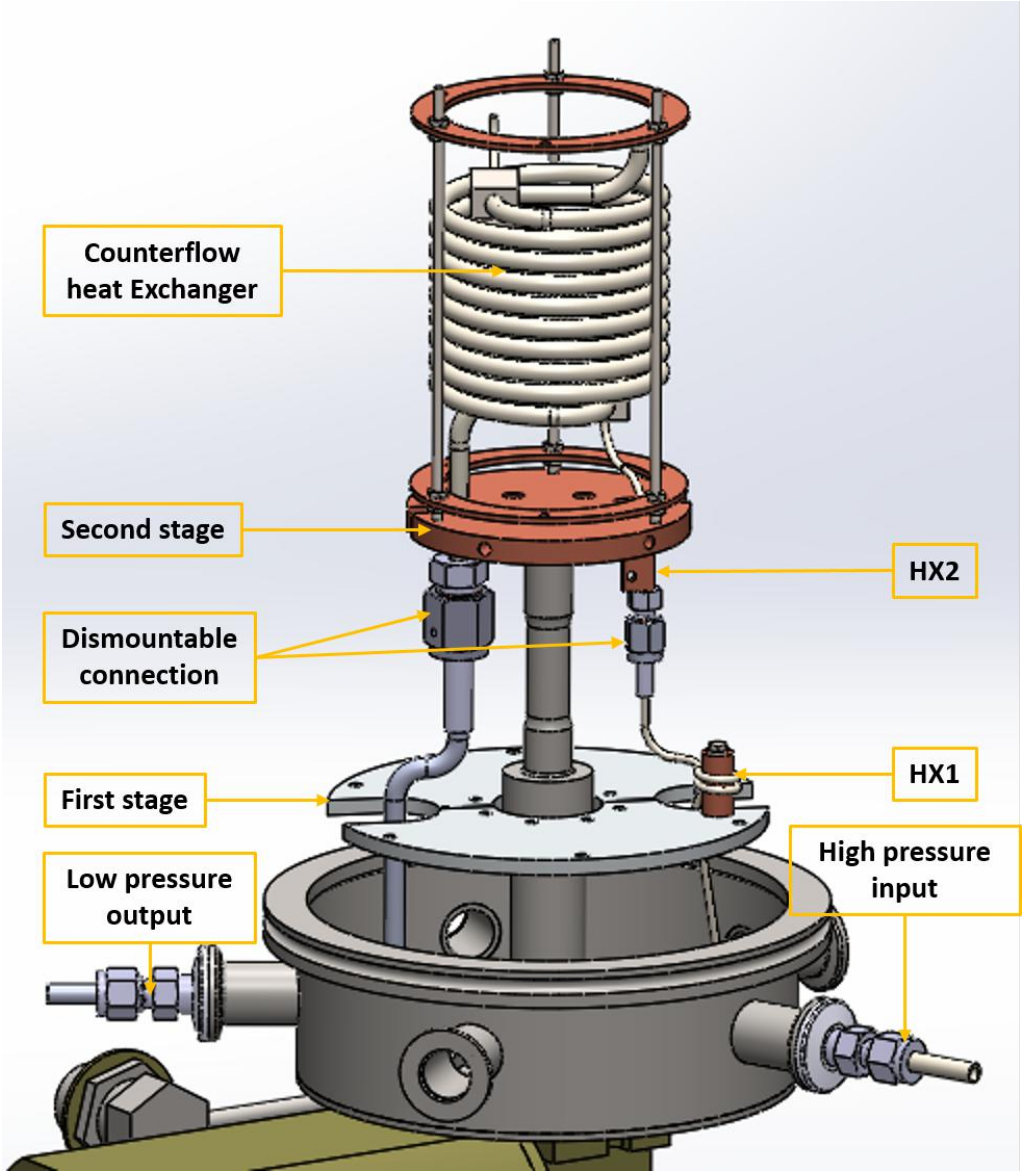

Figure 4.13: SOLIDWORKS drawing for the cold part of the nitrogem JT system

The test system in this the cryocooler was made in a similiar way to that was described in section 4.1.1. However, being this cryocooler smaller, the compactness of the several elements were optimized. Moreover, as far as possible, the various circuit sections are made to be detachable. Then, after all set in the drawing we start building the cold part without a JT valve.

Counterflow heat exchanger

As explained in section 3.2.3 the heat exchanger has a length of 2 m with two tubes, one inside the other (dimensions in table 3.2), in order to turn the heat exchanger more compact these two meters were wounded on a diameter of 60 mm. Similarly to the HX1 manufacturer, to avoid tube crushing, we fill the low pressure tube with salt, instead of water and due to the long length a wire was introduced in the 6 mm tube (low pressure tube) to be used as a guide to allow pulling the high pressure tube through the low pressure one after winding. The winding process is showed in (Figure 4.14).

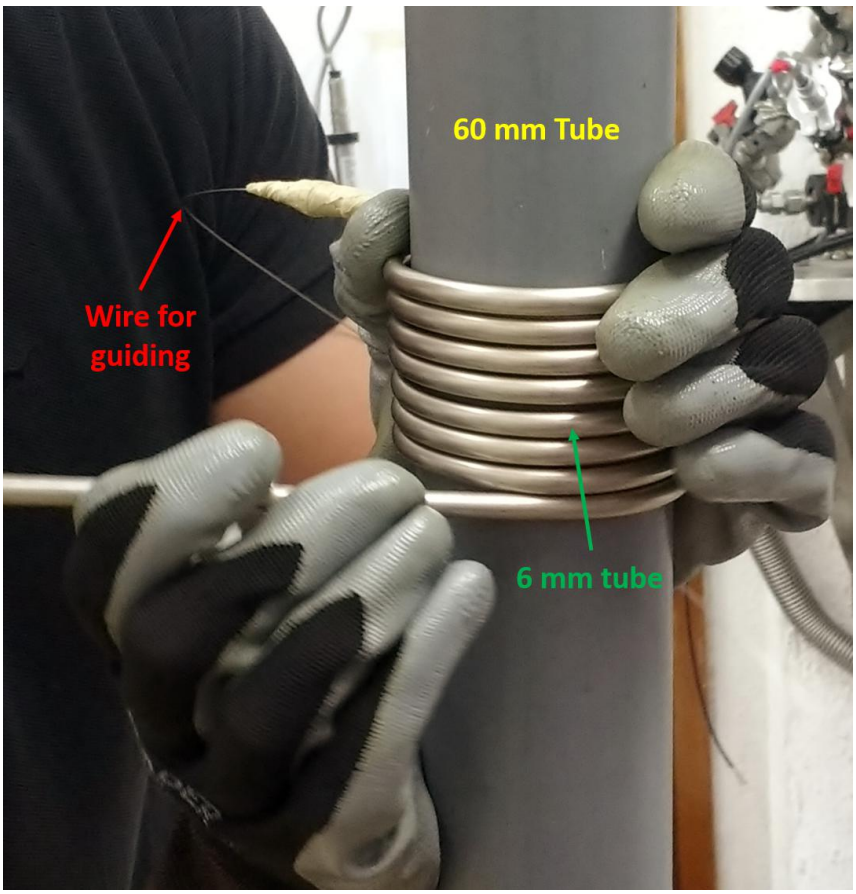

Figure 4.14: The counterflow Heat Exchanger during the winding process

The two extremities of this HX consist on two "splitters" that allow the separation of the HP and LP flow (Figure 4.15) and were manufactured at Physics department workshop (see Appendix. A.1.2).

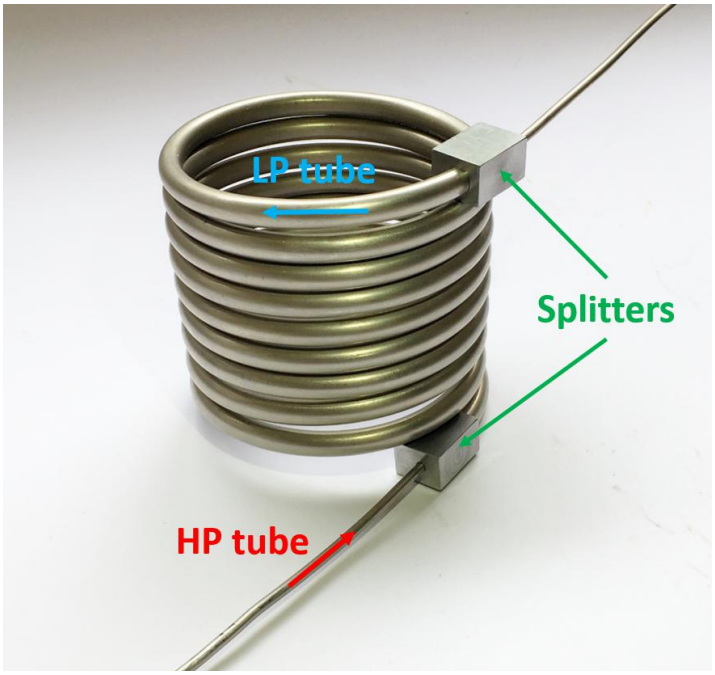

Figure 4.15: The counterflow Heat Exchanger

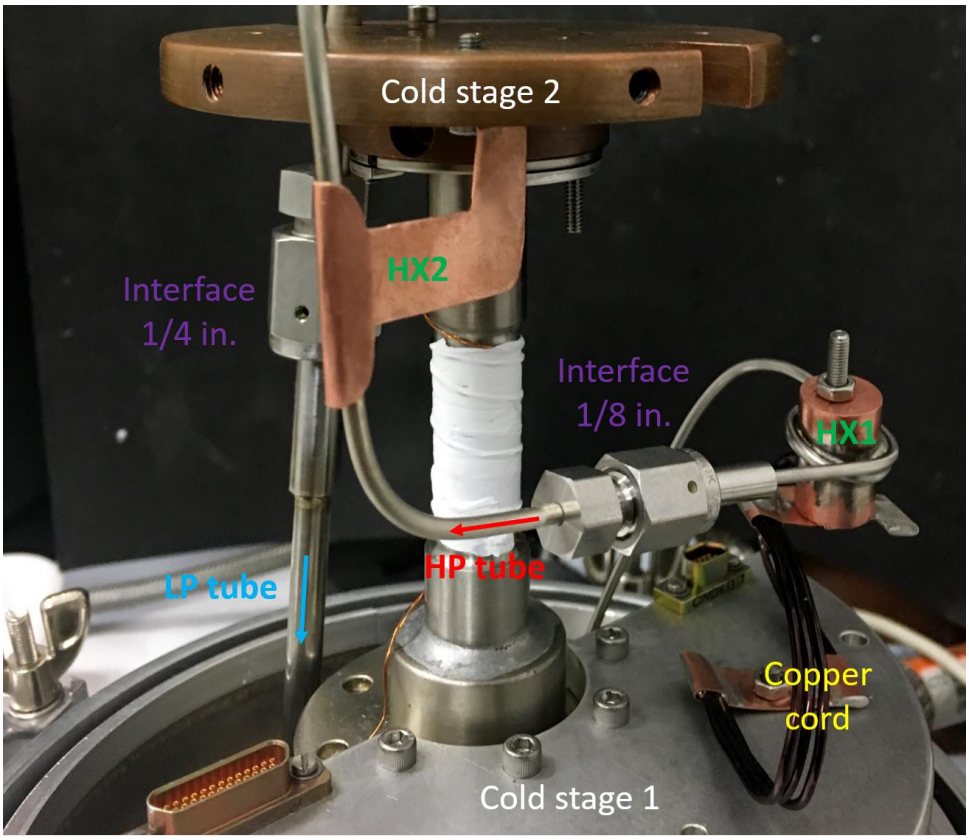

Figure 4.16: HX1 and HX2 for this test system and their thermalizations on stage 1 and 2 of the smaller cryocooler.

The final result is shown in figure 4.17.

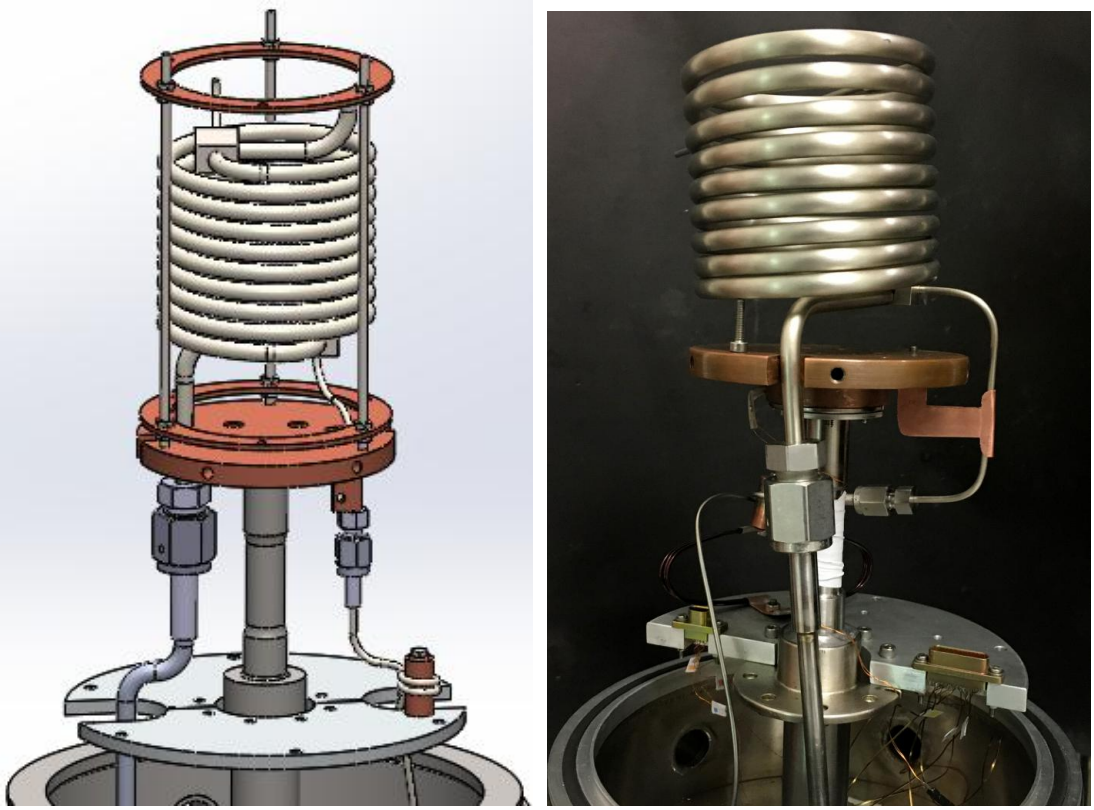

a Projected b Manufactured

Figure 4.17: The Counterflow heat exchanger overall system

Chapter 5

Results and discussion

5.1 Joule-Thomson valve

5.1.1 Mass flow

The first characterization made with Joule-Thomson valve was the determination at room temperature (T = 300 K) of its discharge coefficient, C_d (see in section 4.1). So, we measured the flow under different inlet pressures for both restrictions (49.25 μm and 25.05 μm). The results are displayed in the next plots, the figure 5.1 represents the measured flows and figure 5.2 the discharge coefficients, both calculated using the equation 3.22 and REFPROP data.

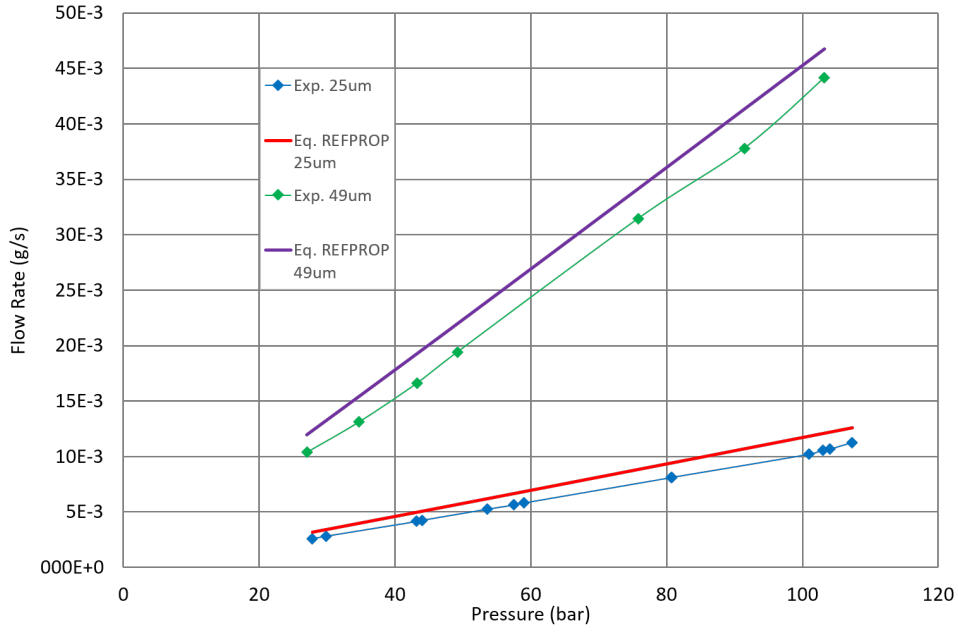

Figure 5.1: The mass flow in function of pressure at room temperature for both restrictions using equation 3.22 and REFPROP data with a C_d of 100%

Through the results we can conclude that on 49.25 μm the mass flow is too high (45 mg/s at 100 bar) and too far from the desired 23.7 mg/s at 100 bar. Also on the 25 μm, the mass flow will be probably too high because the mass flow obtained (13 mg/s) is already near to the objective at room tempetaure, and the decreasing of the temperature to the work temperature will cause an increase of density and a consequently an increase of the mass flow.

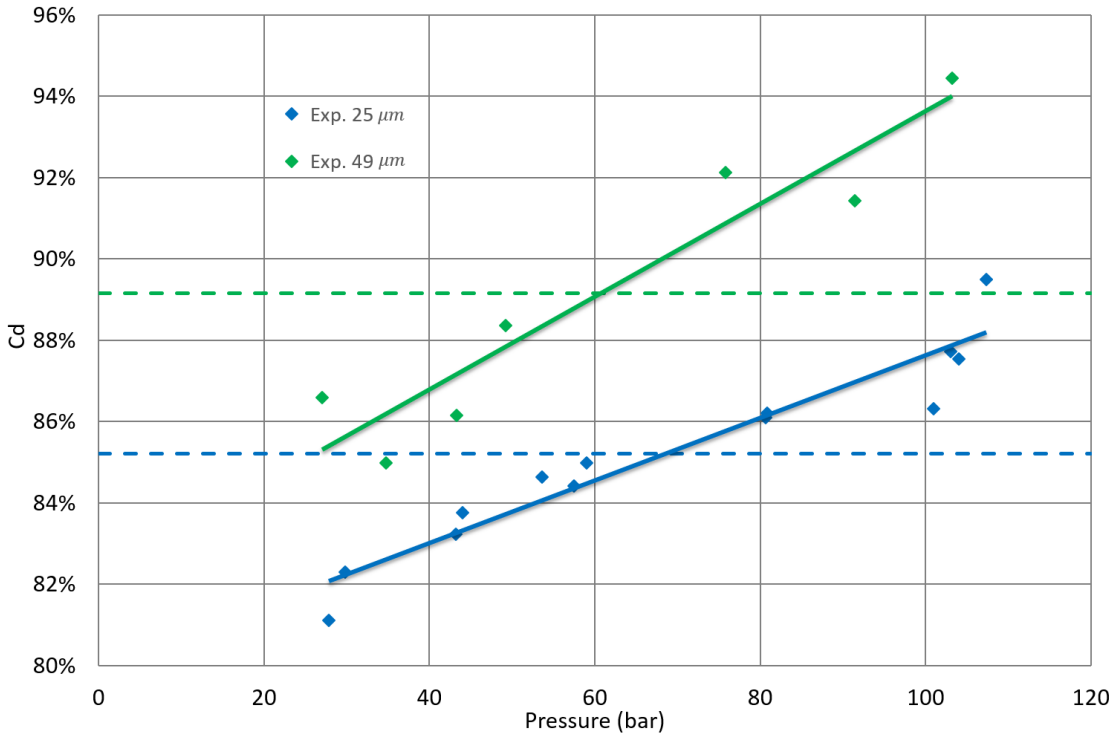

Figure 5.2: The discharge coefficients in function of pressure at room temperature for both restrictions using equation 3.22 and REFPROP data and the dashed lines represents its average value

The figure 5.2 seems to show that the C_d slightly increases with the pressure. However, by a simpler way, it was obtained an average Cd of 85% for the restriction of 25.05 μm and an average C_d of 89% for the restriction of 49.25 μm. Then, we started testing the theoretical equations at lowest temperatures, in order to know if these equations allow us to find the correct orifice diameter for the target mass flow of 23.7 mg/s at 100 bar and 138 K.

But first we had to test our cooling system to see if it was capable to set a stable temperature at the JT valve inlet. As demonstrated in figure 5.3, approximately one hour after introducing the gas and setting the temperatures of the cold stage 2 (Orange line) and HX2 as explained in section 4.1 a stable temperature around 140 K before the Joule-Thomson valve (violet line) was obtained.

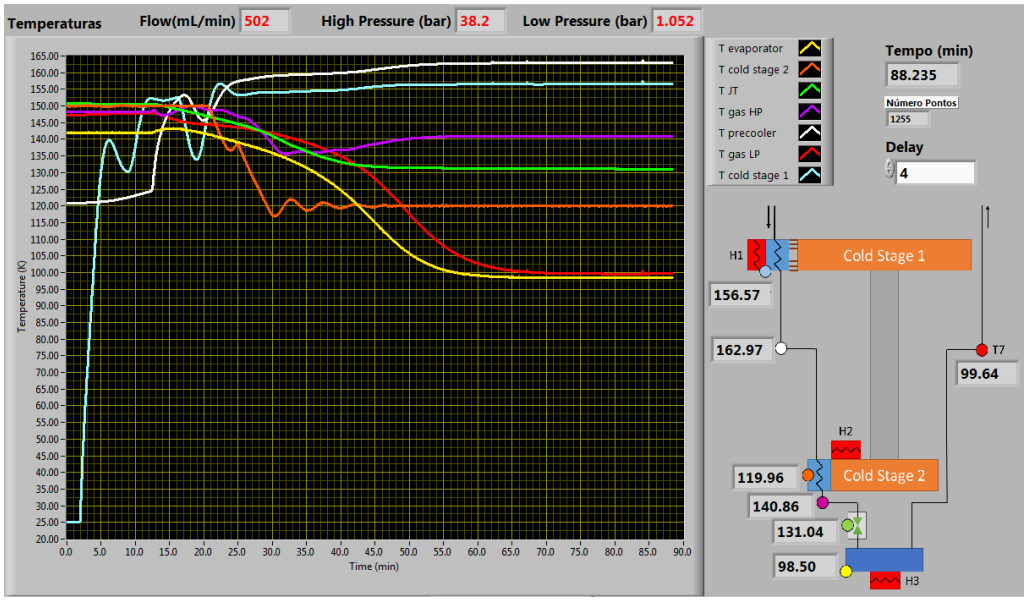

Figure 5.3: Interface of the $LabVIEW^{TM}$ during a test system at 38.2 bar and a mass flow of 502 mL/min. Note the stable temperature of 140.86 K achieved before the expansion (violet line)

So, with the system working it was tested the restriction of 49.25 μm at a fixed pressure of 50 bar and decreasing the inlet Temperature 300 K to 140 K (Figure 5.4) and repeated for the restriction of 25.05 μm at 60 bar (Figure 5.5). In these figures, the experimental results (blue line) are compared to the equation 3.22 with REFPROP data (red line) but also the equation 3.24 for ideal gas (yellow line) and Maytal[12], equation 3.25 (green line).

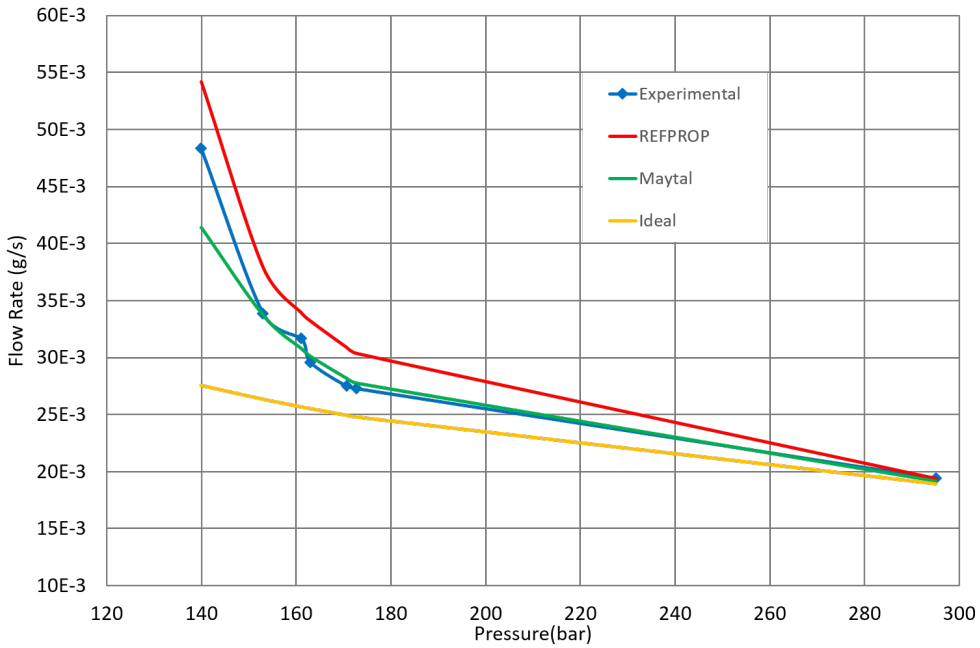

Figure 5.4: The mass flow in function of temperature at a pressure of 50 bar to the restriction of 49.25 μm with a C_d of 89%

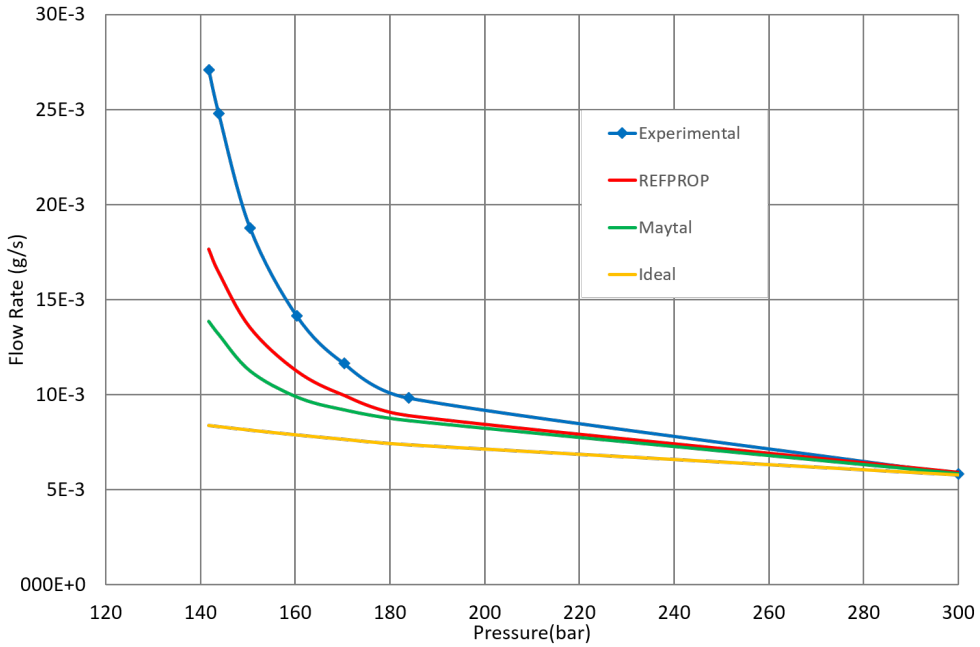

Figure 5.5: The mass flow in function of temperature at a pressure of 60 bar to the restriction of 25.05 μm with a C_d of 85%

In general, the flow increases as T decreases, mainly due to the increase of density. In the plot 5.4 we can observe that when we start decreasing the temperature, the deviations between the theoretical curves and experimental ones increase and the discharge coefficient can no longer correct that differences between them.

It also should be noted that we are with a mass flow much higher than the desired and only in half of the desired pressure. And the flowmeter also has a limitation on the mass flow of around 40 mg/s, so considering this data, we decided to discard this restriction and to work only with the restriction of 25 μm. On the plot of figure 5.5 we had basically the same type of results: discrepancy increase with T and despite the flow being significantly reduced, it is too high in what reffers to our requirements.

But since this orifice was the smallest available at that time, we decided to characterize only this restriction in order to obtain correlations and to compare them with those proposed by Maytal. Then from those correlation obtained, we could dimension the needed diameter of the next restriction with some reliability. So, to optimize time and compare with the Maytal's results, we made the measurements at a constant temperature as a function of pressure and the experimental results are displayed in figure 5.6 ($T_{in} = 151\ K$) and 5.7 ($T_{in} = 141\ K$).

The correlations of factor gamma,Γ, are obtained dividing the experimental results obtain for the mass flow by the calculations for the mass flow in a ideal gas. These results are replotted as a function of Π_0 ($P/P_c, P_c = 34bar$) and for the two different Θ_0 ($T/T_c, T_c = 126K$), those are represented in figure 5.8, the curves blue and red represent our values to Γ at 141 K and 151 K, respectively.

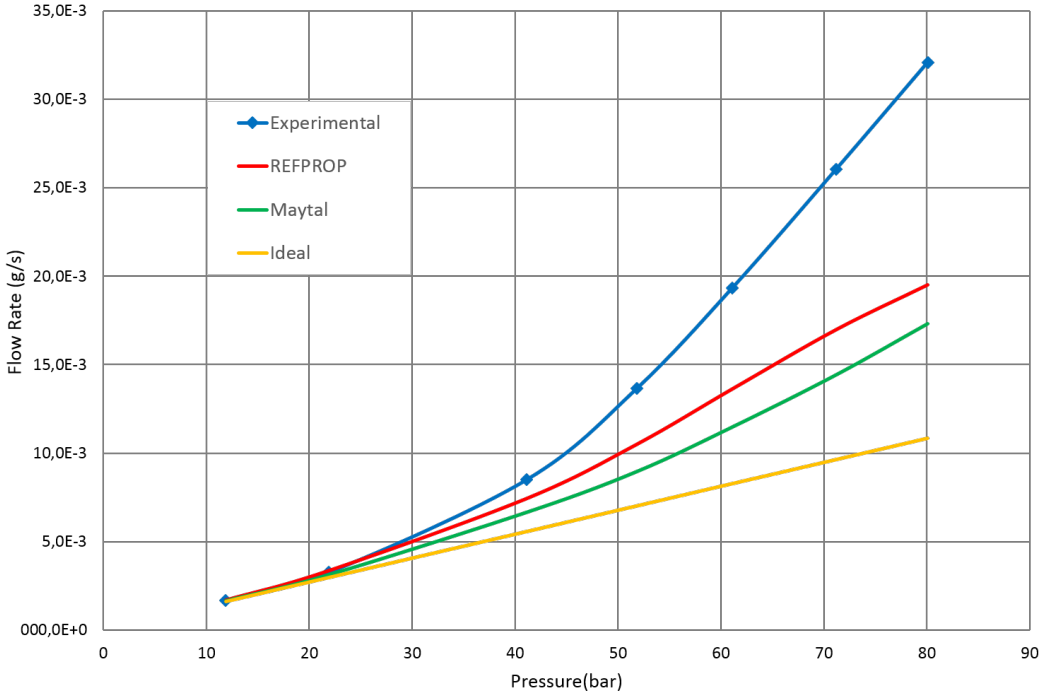

Figure 5.6: The mass flow in function of pressure at a temperature of 151 K to the restriction of 25.05 μm with a C_d of 85%

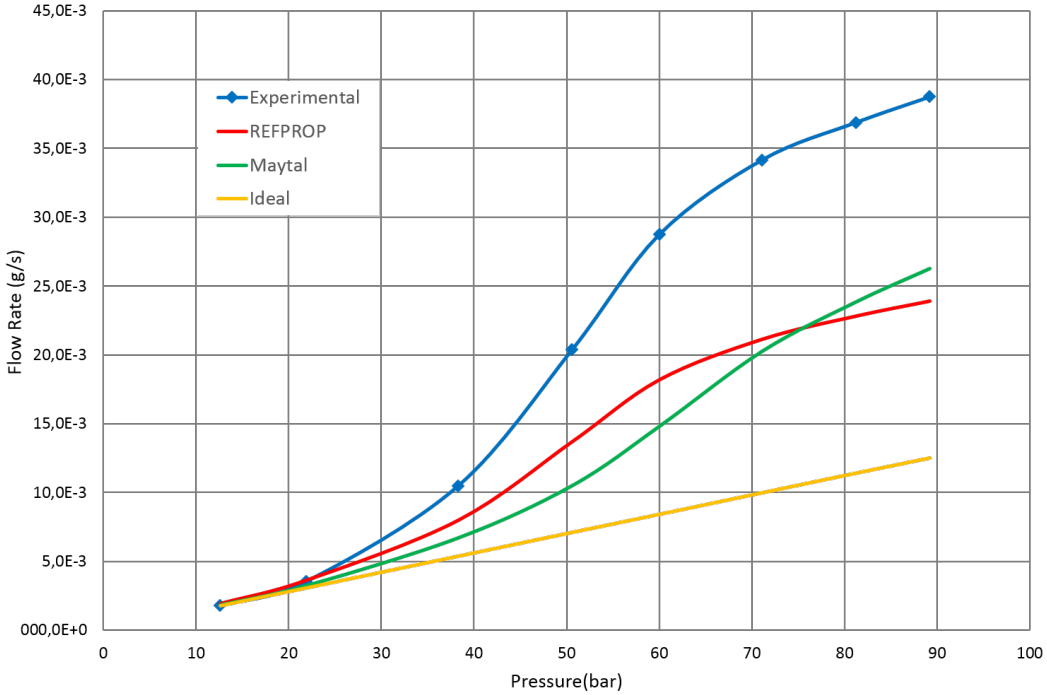

Figure 5.7: The mass flow in function of pressure at a temperature of 141 K to the restriction of 25.05 μm with a C_d of 85%

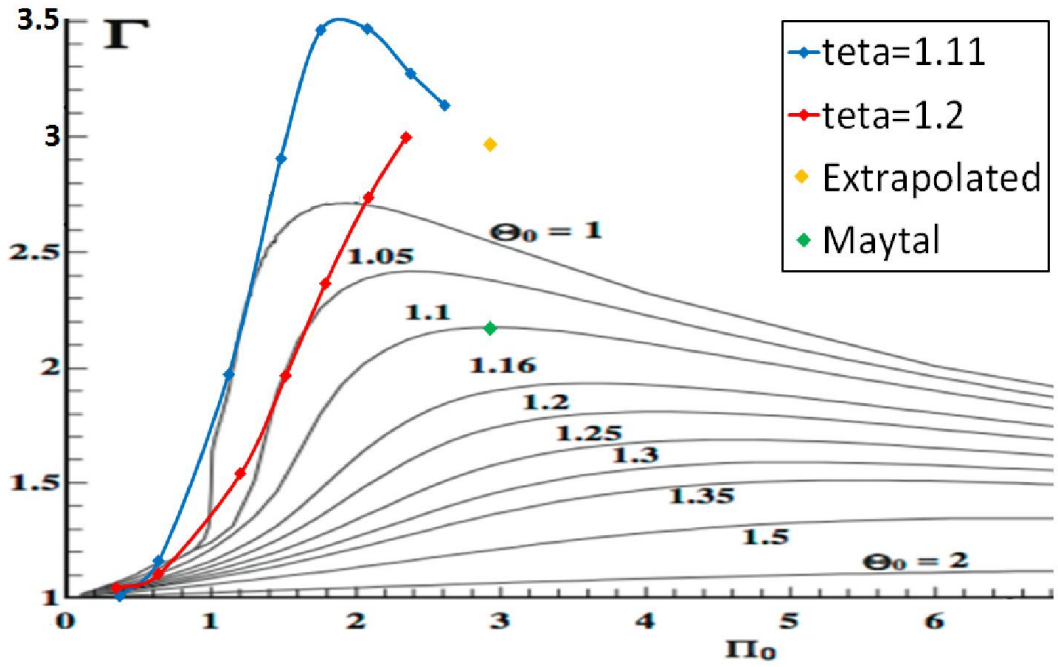

Figure 5.8: Comparison of the Maytal's correction factor Gamma[12] and our results. Black lines: Maytal's results, red line: 151 K; blue line: 141 K, yellow point: extrapolated and green point Maytal's result both under our work conditions

Once again the flows were already too high at 90 bar and 141 K, very close to the highest detection limit of the flow meter. That is why we could not get closer of the work conditions but in order to determine the appropriate diameter for the orifice using the equation 3.25, we had to obtain the gamma factor to ours work conditions from the previous curves. So, to do that we had to extrapolate a gamma for these conditions, $\Pi_0 = 2.94$ and $\Theta_0 = 1.10$,

$$\Gamma^* = 2.93 \tag{5.1}$$

and under our work conditions by Maytal's correlation:

$$\Gamma = 2.15 \tag{5.2}$$

So we used both correlations to have an idea of the restrictions diameter. The results are indicated in table 5.1.

Table 5.1: The predicted diameters for a flow of 23.7 mg/s

Γ	Diameter (μm)	
$\Gamma = 2.15$	18.2 ($C_d = 100\%$)	19.5 ($C_d = 87\%$)
$\Gamma^* = 2.93$	15.6 ($C_d = 100\%$)	16.7 ($C_d = 87\%$)

5.1.2 Thermodynamic of the cold part

Despite of the fact that the target flow conditions were not obtained with the smallest orifice, we tested if, in the available conditions of temperature and pressure with the 25 microns orifice, the results obtained after the JT expansion were in agreement with those expected from thermodynamics.

To test the isenthalpic expansion in the Joule-Thomson valve we used the case with a fixed pressure of 60 bar for five different T_{in} (Figure 5.5). These are represented on the PH diagram (Figure 5.9) and the results are demonstrated in table 5.2.

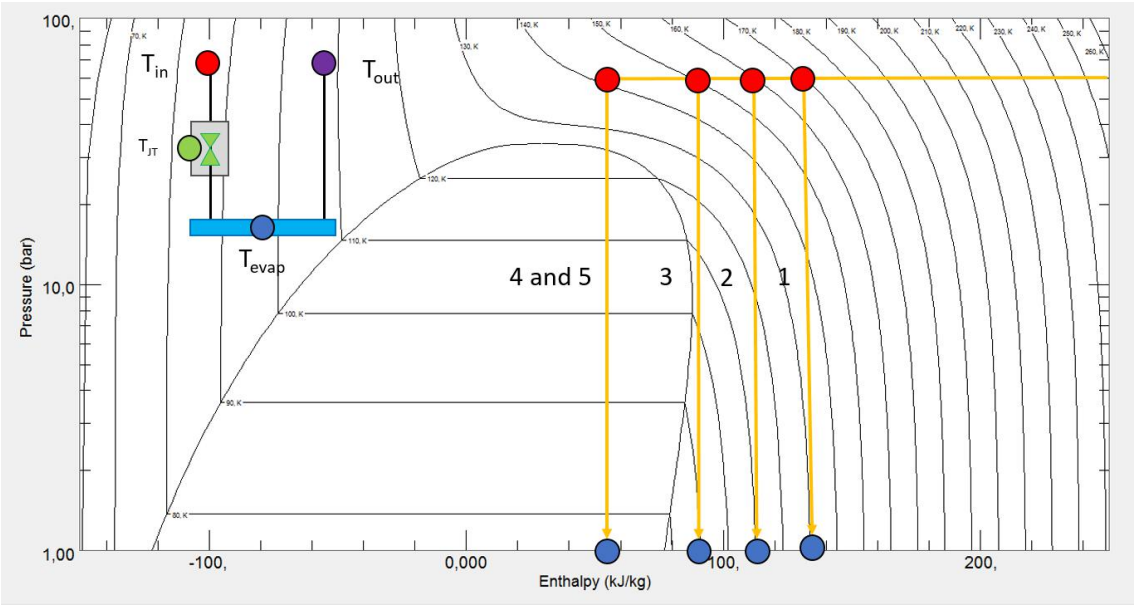

Figure 5.9: Representation of the isenthalpic expansion in the Joule-Thomson valve at 60 bar.

Table 5.2: Results of the isenthalpic expansion at 60 bar. T_{in}, T_{JT} and T_{evap} correspond respectively to T_4, T_5 and T_6 in figure 4.3. $T_{expexted}$ is obtained from the PH diagram of figure 5.9

$n°$	$\dot{m}(mg/s)$	$T_{in}(K)$	$T_{JT}(K)$	$T_{evap}(K)$	$T_{expected}(K)$
1	12	170	153	130	129
2	14	160	146	112	111
3	19	150	140	90	89
4	26	144	135	77.5	77.8
5	27	142	132	77.4	77.8

As demonstrated on the table above the error between the temperature of the evaporator and the expected temperature is always below 1%. That proves that our experimental setup for the JT valve seems to work perfectly.

A second test consists on checking if the cooling power is in agreement with our calculations.

To calculate the cooling power that we are capable of producing we need to be on a situation where we are producing liquid nitrogen on the evaporator. Then the cooling power corresponds to the heating power needed to evaporate exactly the liquid quantity formed after the JT expansion.

For example if we choose the point 5 of the table 5.2, a quite high power has to be applied in order to make sure that we are evaporating all the liquid and then start decreasing this power until we get a balance between the liquid nitrogen that is formed and the evaporated.

A way to see this process is through the temperatures (Figure 5.10), when we apply a power higher than a cooling power we also are increasing the temperature of thermometers nearby, like T_{out}. Therefore, when the T_{out} is equal to T_{evap} means that we are in the balance. It is clear that if we continue to decrease the power, the temperatures will remain the same because we are accumulating liquid, that is why we need to start in a higher power applied. The temperature versus the applied power as plotted in figure (Figure 5.11).

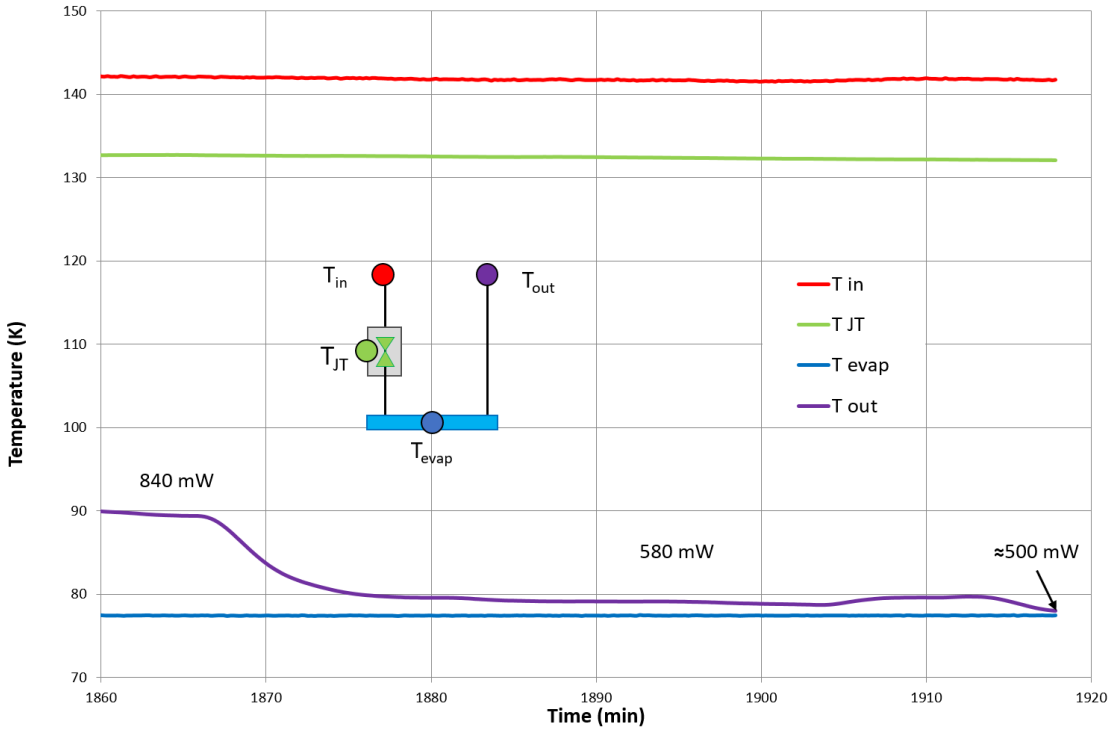

Figure 5.10: Variation of the temperatures during the process used for cooling power (CP) determination (See text) at a pressure and heating power (H3, see figure 4.3) constant

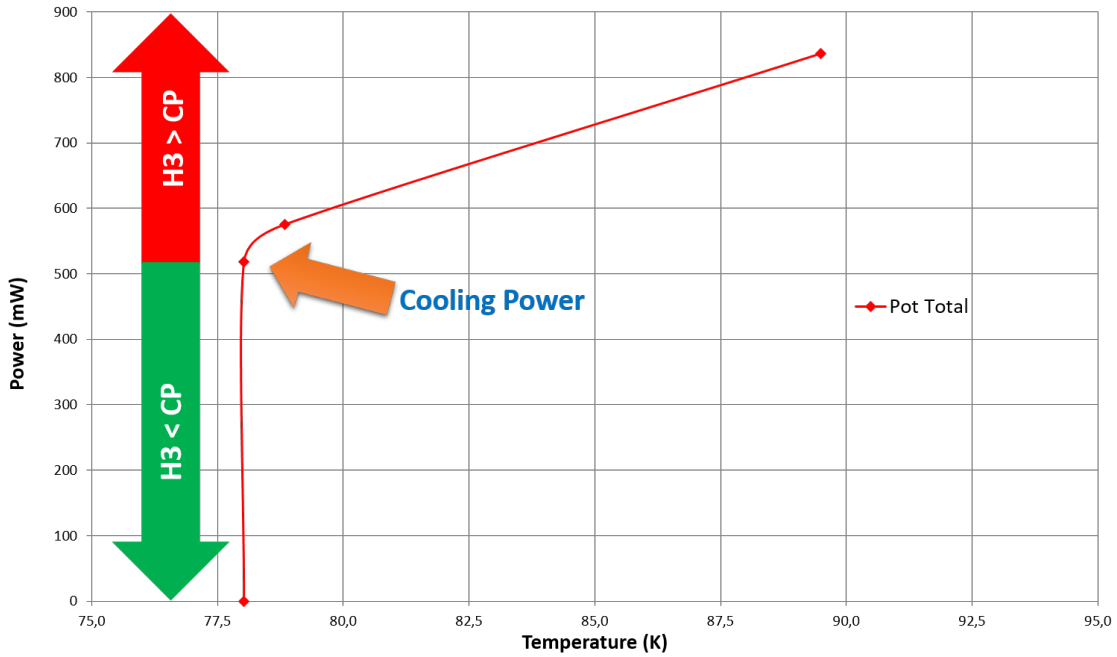

Figure 5.11: Dependence of T_{out} and heating power applied (H3) during the process of cooling power (CP) determination.

As demonstrated we obtained a cold power of around 500 mW. The theoretical cold power corresponding to this thermodynamic process can be calculated using the equation 3.2,

$$\dot{Q} = 27 \times 10^{-3}(H_{60bar,142K} - H_{1bar,78K}) \approx 500mW \tag{5.3}$$

This good agreement between expected results and those obtained demonstrates that our measurements system is working perfectly without any flaws and it also proves that the JT expansion occurring in this system fulfills its expected role.

Chapter 6

Conclusions

This thesis had as main objective the construction and characterization of the cold part of a 80 K vibration-free cooler.

Due to technical and temporal reasons, this main objective was splitted in two. Both were essential, one of them was the characterization of the Joule-Thomson restrictions and the construction of the respective test system, capable of precooling the flow down to the required temperature (138K); the other objective was the dimensioning of the counterflow Heat Exchanger and its construction.

The system to precool the flow was mounted in a already existing cryocooler and it was a success: we were able of setting a desired temperature at the entrance of the Joule-Thomson valve with high accuracy. This system allowed us to obtain the flow to characterize the restrictions for several temperatures and pressures.

The results showed that our restrictions were too large since the mass flows obtained exceeded the target conditions: the 25 mg/s flow was obtained at 142 K with a pressure of 60 bar instead of 100 bars using the restriction with a diameter of 25 μm. We also found out that there is a significant difference between the results and the expected mass flows for ideal gases, using REFPROP data and Maytal's correlations. This difference increases as the inlet temperature decreases and not even with the Maytal's model we could reproduce our results. This error could be due to the irregularity of the restriction geometry made by the laser, as demonstrated in SEM pictures. If that is the case, the right orifice, leading to the target conditions, will be obtained by try and error. However, now with the correlation obtained, we can extrapolate some possible diameters for the orifice (Table 5.1). So, for our mass flow we need a diameter around 17 μm. The new orifices were ordered recently and will be tested in the near future.

With the system built during this thesis, the determination if the new orifices are the right ones can be made quickly and easily, not only for this project but for any project of this type.

In what refers to the thermodynamic part of Joule-Thomson expansion, the experimental results are in great agreement with the expected ones. The error between the experimental results and the expected results was less than 1 %.

In addition the results of the cooling power that we got also were in agreement with the cooling power expected.

Although, we were not at targeting conditions, this assures us the performances expected from the thermodynamics will be obtained with a great degree of reliability, a cold power of 1.5 W at a temperature around 80 K.

The dimension of the counterflow heat exchanger was obtained using classical calculation for these types of heat exchangers. This was built according to this dimensioning and the winding step it was also successful. The test system is practically assembled, by simply adding the correct Joule-Thomson valve, the system is complete and then it will be possible not just to test the Counterflow Heat Exchanger but also the entire cold stage. From the Joule-thomson system to the counterflow heat exchanger we made some improvements such as the introduction of demountable interfaces without desoldering, which brought some problems on the previous system like clogging.

Although, we had not the opportunity to test the Counterflow Heat Exchanger, I think it will work perfectly because we had more half meter at it is length to ensure its working.

As a conclusion I would like to mention that since all of the main objectives were accomplished this master thesis was a success. Despite all obstacles, in a future, we will be able to create the 40-80 K vibration-free cooler that will be essential for the operation of high resolution sensors by eliminating all of the vibrations that are caused by the majority of the cryocoolers already existing. In addition I would like to emphasize that the realization of this project was a great asset for me once I had the opportunity of working at this innovative programme in the Lab of Cryogenics which taught me so much.

Bibliography

[1] *Cryocoolers for space applications — Cryogenic Engineering Group, University of Oxford*. [Online]. Available: http://www.eng.ox.ac.uk/cryogenics/research/cryocoolers-for-space-applications (visited on 11/15/2015).

[2] D Pearson, B Zhang, M Prina, and C Paine, "Flight Acceptance Testing of the Two JPL Planck Sorption Coolers", pp. 497–504, 2007.

[3] G Morgante, D Pearson, F Melot, P Stassi, L Terenzi, P Wilson, L Wade, A Gregorio, M Bersanelli, C Butler, and N Mandolesi, "Cryogenic Characterization of the Planck Sorption Cooler System Flight Model", pp. 1–18, 2008.

[4] P. C.P.A. R. Ade, N Aghanim, M Arnaud, M Ashdown, J Aumont, and C Baccigalupi, "Special feature Planck early results . II . The thermal performance of Planck", vol. 2, 2011.

[5] Y Wu, T Mulder, C. H. Vermeer, H. J. Holland, B Benthem, and H. J. M. Brake, "Vibration-free cooler for the METIS instrument using sorption compressors", vol. 67, pp. 411–416, 2015. DOI: 10.1016/j.phpro.2015.06.050.

[6] F. P. Incropera and D. P. DeWitt, *Fundamentals of Heat and Mass Transfer*, 6 th. 2002, ISBN: 9780471457282.

[7] J. Case and A. Chilver, *Strength of Materials and Structures*, 1971. [Online]. Available: http://www.sciencedirect.com/science/book/9780340719206.

[8] E. HEARN, *Mechanics of Materials 1*. Elsevier, 1997, pp. 215–253, ISBN: 9780750632652. DOI: 10.1016/B978-075063265-2/50011-6. [Online]. Available: http://www.sciencedirect.com/science/article/pii/B9780750632652500116.

[9] *Thermodynamics and Propulsion, Prof. Z. S. Spakovszky, MIT*. [Online]. Available: http://web.mit.edu/16.unified/www/FALL/thermodynamics/notes/notes.html (visited on 12/20/2015).

[10] B.-Z. Maytal and J. M. Pfotenhauer, *Miniature Joule-Thomson Cryocooling*, 1 th. 2013, ISBN: 9781441982858.

[11] E. Lemmon, M. L. Huber, and M. O. McLinden, *NIST Standard Reference Database 23: Reference Fluid Thermodynamic and Transport Properties, version 9.1*, Gaithersburg, 2013.

[12] B.-z. Maytal and E. Elias, "Two-phase choking conditions of real gases flow at their critical stagnation temperatures and closely above", *Cryogenics*, vol. 46, no. 9, pp. 21–29, 2006, ISSN: 0011-2275. DOI: 10.1016/j.cryogenics.2005.09.003. [Online]. Available: http://dx.doi.org/10.1016/j.cryogenics.2009.06.009.

APPENDIX

A.1 Cold stage system in SOLIDWORKS

A.1.1 Drawings

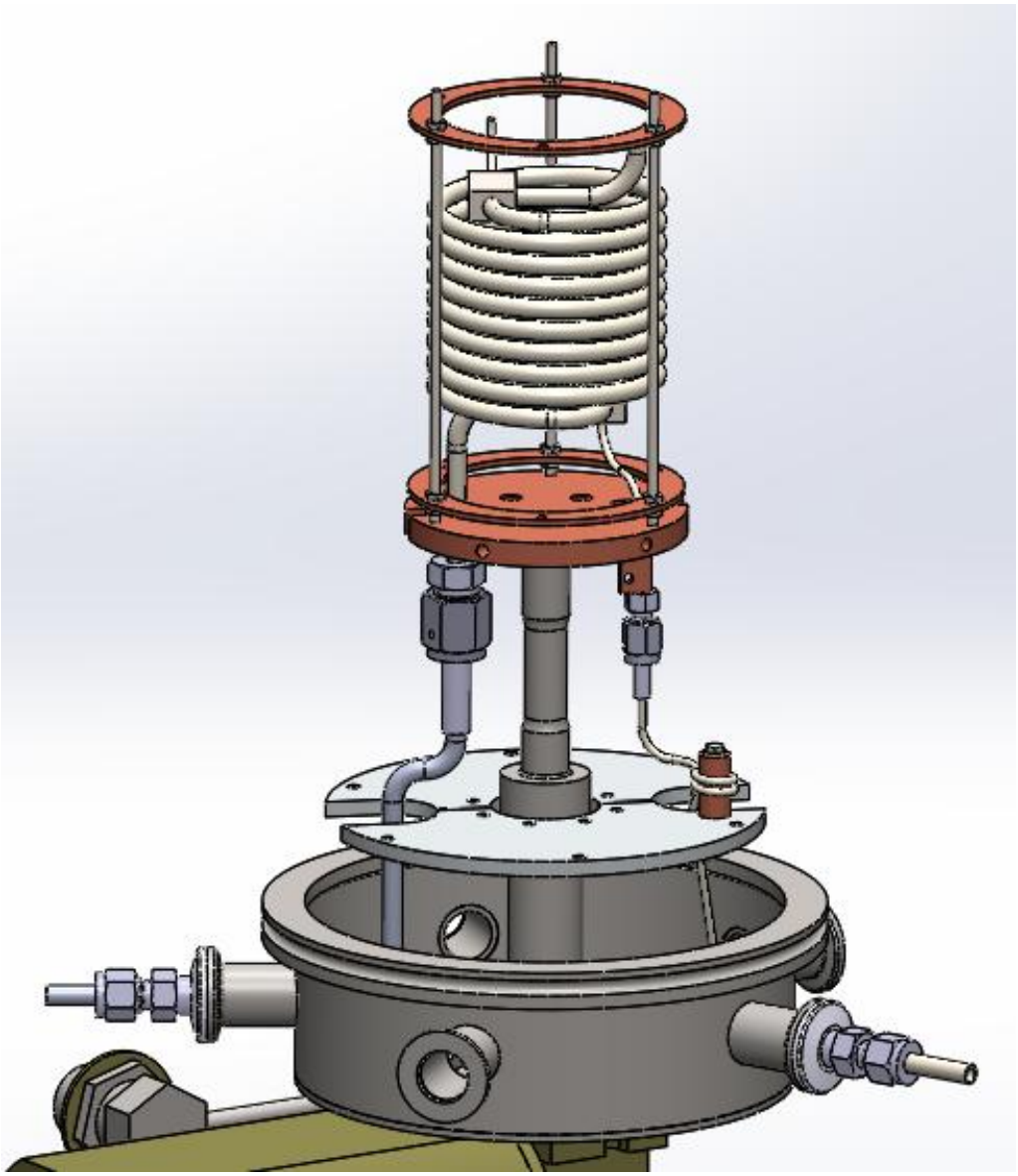

Figure A.1: Overall system

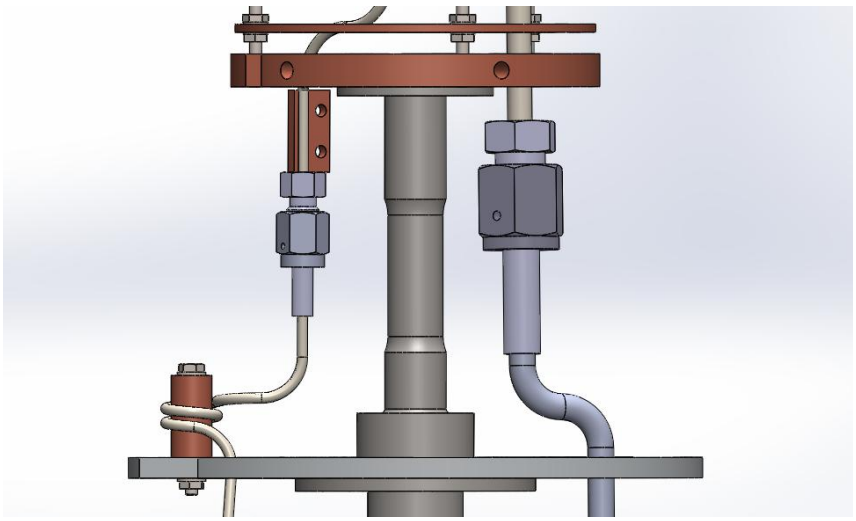

Figure A.2: Precooling system and internal interfaces

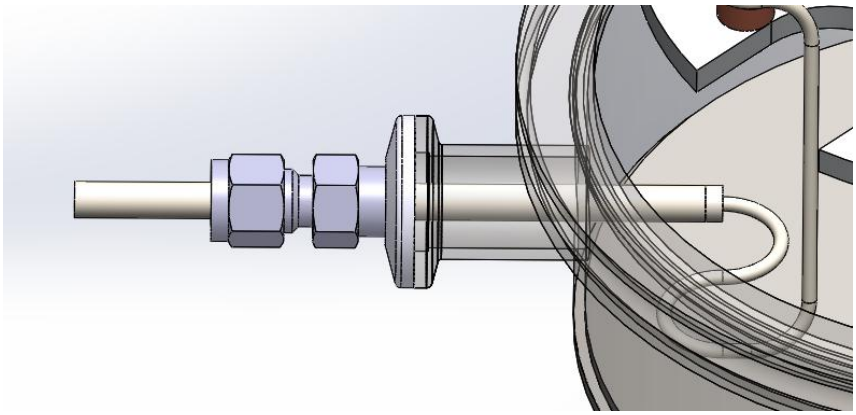

Figure A.3: High pressure interface with the outside of the cryocooler

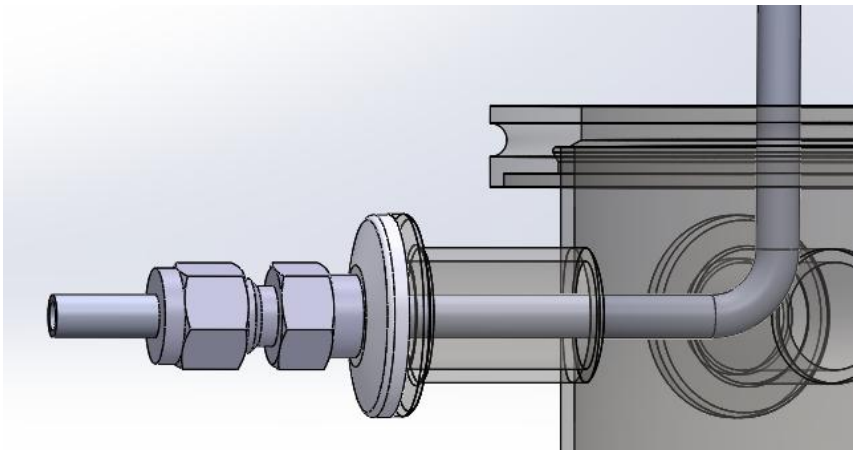

Figure A.4: Low pressure interface with the outside of the cryocooler

A.1.2 Technical drawings

REV.	DATE

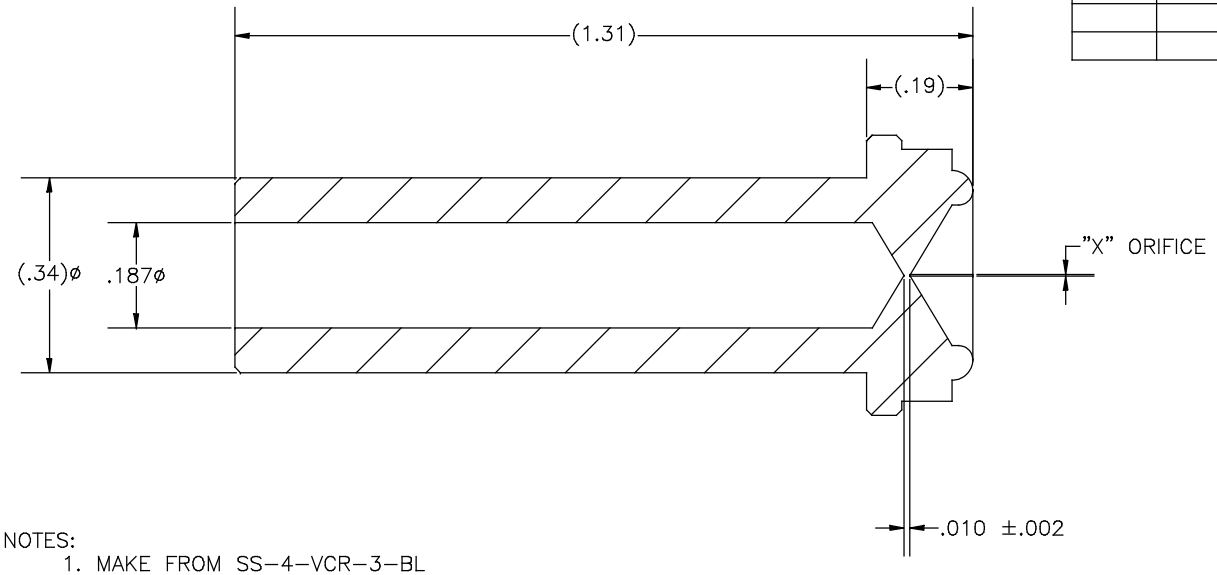

NOTES:

1. MAKE FROM SS-4-VCR-3-BL
2. DRILLED FOR 1/4" TUBING OR BUTT-WELDING.

UNLESS OTHERWISE SPECIFIED DIMENSIONS ARE IN INCHES ANGLES± 0°-30' DECIMALS .XX ± .02 .XXX ± .005	SS-4-VCR-3-X
	LENOX LASER BY FRH INITAL RELEASE 11-15-06

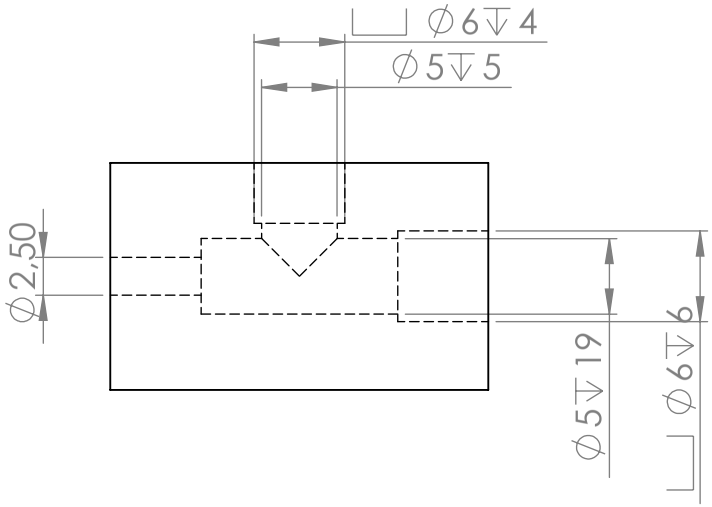

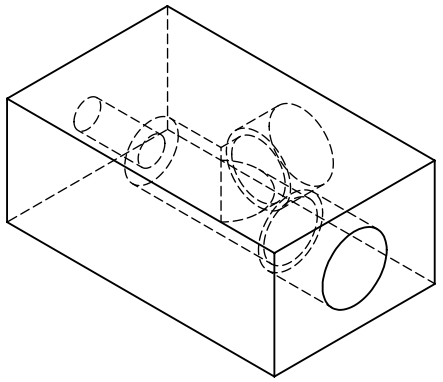

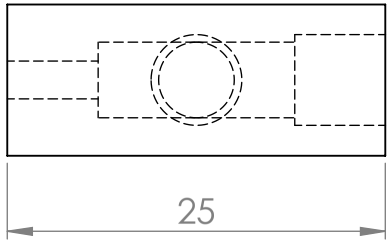

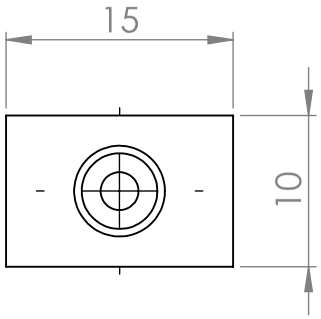

	Nome	Data
Desenho	MB	15/03/16
Verificação	GB	15/03/16

MATERIAL: Stainless steel

Peça: **Steel block to separate fluids**

Lab. Criogenia FCT-UNL

Tamanho: A4

Escala: 2: 1

Tolerância: X:±0.1

Nome desenho: Splitter

1 peça

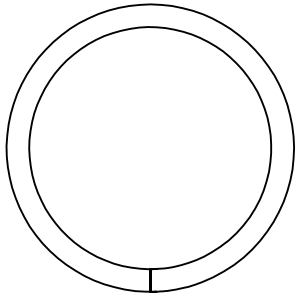

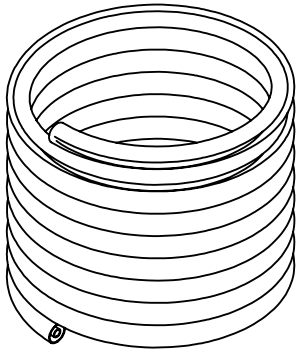

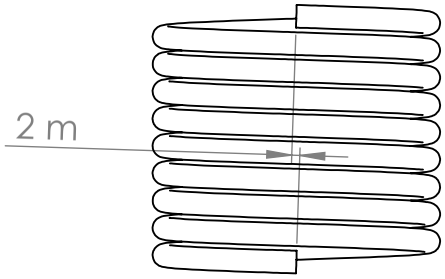

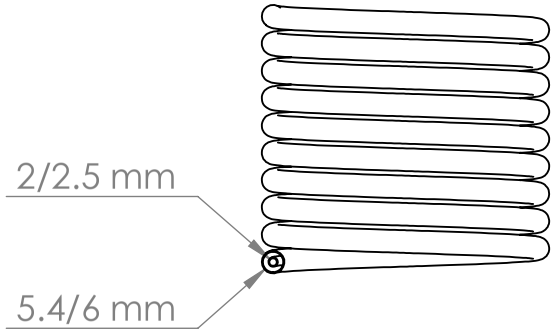

	Nome	Data
Desenho	MB	15/03/16
Verificação	GB	15/03/16

MATERIAL: Stainless steel

Peça: **Counterflow Heat Exchanger**

Lab. Criogenia FCT-UNL

Tamanho: A4

Escala: 2 : 1

Tolerância: X:±0.1

Nome desenho: **Counterflow Heat Exchanger**

1 peça